A Framework to Simulate Small Shallow Inland Water Bodies in Semi-arid Regions

Abbasi, Ali; Annor, Frank; van de Giesen, Nick

DOI
10.1016/j.advwatres.2017.09.023

Publication date
2017

Document Version
Final published version

Published in
Advances in Water Resources

Citation (APA)
Abbasi, A., Annor, F., & van de Giesen, N. (2017). A Framework to Simulate Small Shallow Inland Water Bodies in Semi-arid Regions. *Advances in Water Resources*, *110*, 77-96. https://doi.org/10.1016/j.advwatres.2017.09.023

Advances in Water Resources 110 (2017) 77–96

Contents lists available at ScienceDirect

Advances in Water Resources

journal homepage: www.elsevier.com/locate/advwatres

A framework to simulate small shallow inland water bodies in semi-arid regions

Ali Abbasi[*,a,b], Frank Ohene Annor[b,c], Nick van de Giesen[b]

[a] Civil Engineering Department, Ferdowsi University of Mashhad, P.O. Box 91775-1111, Mashhad, Iran
[b] Department of Water Resources, Faculty of Civil Engineering and Geosciences, Delft University of Technology, Stevinweg 1, 2628 CN, Delft, Netherlands
[c] Civil Engineering Department, Kwame Nkrumah University of Science and Technology, Kumasi, Ghana

ARTICLE INFO

Keywords:
Shallow water bodies
Semi-arid regions
Complex bathymetry
OpenFOAM
Lake heat storage

ABSTRACT

In this study, a framework for simulating the flow field and heat transfer processes in small shallow inland water bodies has been developed. As the dynamics and thermal structure of these water bodies are crucial in studying the quality of stored water , and in assessing the heat fluxes from their surfaces as well, the heat transfer and temperature simulations were modeled. The proposed model is able to simulate the full 3-D water flow and heat transfer in the water body by applying complex and time varying boundary conditions. In this model, the continuity, momentum and temperature equations together with the turbulence equations, which comprise the buoyancy effect, have been solved. This model is built on the Reynolds Averaged Navier Stokes (RANS) equations with the widely used Boussinesq approach to solve the turbulence issues of the flow field. Micrometeorological data were obtained from an Automatic Weather Station (AWS) installed on the site and combined with field bathymetric measurements for the model. In the framework developed, a simple, applicable and generalizable approach is proposed for preparing the geometry of small shallow water bodies using coarsely measured bathymetry. All parts of the framework are based on open-source tools, which is essential for developing countries.

1. Introduction

Inland water bodies, especially small lakes and reservoirs, are used extensively throughout the world to store water for irrigation purposes, municipal water supply, recreation, and water treatment (Lee, 2007). In this study “small shallow lake” represents the inland water body with a surface area between 1.0 and 100 ha and a maximum depth of 5.0 m. The ability of these water bodies to function depends on the conditions within the water body, which can be influenced by the flow conditions and the temperature distribution. Understanding the conditions existing within shallow water bodies calls for details of the flow through the water body, obtained either by measuring the flow parameters and temperature distribution or simulating the processes of stratification and circulation in the water body. Stratification in a water body prevents mixing of water temperatures, dissolved substances, and nutrients within the water column and can impose additional impacts on the water quality and ecological health of the water body. In most cases, carrying out measurements over small shallow inland water bodies is difficult and expensive, demanding a high level of expertise to obtain reliable measurements over the water surface even for measuring conventional micrometeorological variables such as air temperature and wind velocity.

Accurate estimation of airflow and heat exchanges at the air-water interface in shallow reservoirs is vital for studying the heat, moisture, and momentum transfers between a water surface and its atmospheric boundary layer above. In shallow inland water bodies, the near-surface water temperature commonly follows the radiative forcing (solar radiation) trend with an increase during the day and a decrease during the night. The temperature gradient can move vertically into the water column by (effective) thermal diffusivity, which can be enhanced by the atmospheric parameters, water surface waves and the dynamics of the flow in the water body (Vercauteren et al., 2011; Yang et al., 2016). Eddy diffusivity and thermal conductivity are important parameters in simulating the diurnal evolution of the temperature in these water bodies (Yang et al., 2016). Wind over water surface affects lake currents, sensible and latent heat fluxes and turbulence as well as surface waves. The time-dependent effects of wind shear stress over the flow can change the flow pattern and thermodynamics of the lake. Therefore, the effects of heat transfer and wind-induced flow in small shallow water bodies is complicated and needs the use of high-resolution

* Corresponding author.
E-mail addresses: a.abbasi@tudelft.nl (A. Abbasi), annorfrank@yahoo.co.uk (F. Ohene Annor), n.c.vandegiesen@tudelft.nl (N. van de Giesen).

http://dx.doi.org/10.1016/j.advwatres.2017.09.023
Received 10 July 2016; Received in revised form 22 August 2017; Accepted 26 September 2017
Available online 05 October 2017

simulation to determine the flow variables.

During the last decades a large number of models with a wide range of complexity, from simple one-dimensional models to full three-dimensional circulations models, have been produced. There is a wide range of one-dimensional models (e.g. Dynamic Reservoir Simulation Model (DYRESM), Fresh-water Lake model (FLake), etc.) with different assumptions, numerical methods and performance abilities in simulating inland water bodies (FLake, 2016). These models assume one-dimensionality conditions for the flow, where the scale of heat and momentum changes in vertical direction (depth) is commonly much larger than in the horizontal directions (Abeysinghe et al., 2005; Gooseff et al., 2005; Han et al., 2000; Herb and Stefan, 2005; Hondzo and Stefan, 1993; Kirillin, 2002; 2010). Although this simplification makes the model more straightforward, some significant complex processes that occur in the water bodies, especially in shallow ones, are ignored. However, 1-D models remain attractive due to their appropriateness, simplicity and convenience for studying the flow and temperature dynamics in deep and large reservoirs, especially for long-term simulations (Abeysinghe et al., 2005). In general, 1-D models cannot be used to predict thermal stratification in shallow water bodies where the horizontal advective term cannot be neglected.

Two-dimensional models are widely used for studies on inland water bodies. They are based on depth-averaged equations commonly known as shallow water equations. In 2-D models, it is assumed that the vertical length scale is much smaller than the horizontal, hence a hydrostatic pressure distribution is assumed, which significantly simplifies the numerical formulation and computational implementation (Bednarz et al., 2008; 2009; Kim and Cho, 2006; Lap and Mori, 2007; Lee, 2007; Lei and Patterson, 2001; 2002; Naithani et al., 2007).

It has been recognised that the vertical direction plays a significant role in the circulation of shallow water bodies which one- and two-dimensional models are unable to simulate (Vreugdenhil, 1994). The flow parameters in shallow water bodies typically have a three-dimensional structure due to the effects of complex bathymetry and temperature (density) stratification (Lee, 2007). From the field measurements carried out by Sweeney (2004), the water bodies with one meter depth or even less can become thermally stratified. A number of three-dimensional models (e.g. MIT General Circulation Model (MITgcm), Estuary and Lake Computer Model (ELCOM)) have been developed and used by some authors to study the 3-D flow structures of shallow water bodies (Appt et al., 2004; Fan and Furbo, 2012; Hodges and Dallimore, 2014; Koçyigit and Falconer, 2004; Laval et al., 2003; Lee et al., 2009; Lee, 2007; Liu et al., 2012; Marshall et al., 1997; MITgcm, 2016; Sweeney, 2004; Ta and Brignal, 1998; Yamashiki et al., 2003).

Investigation of the studies discussed above revealed that several difficulties were encountered in using them in modeling small shallow lakes. The main reasons for this can be summarized as follows:

1. these models have been developed mainly for large and deep lakes where the impacts of the boundary conditions on the flow field and temperature dynamics could be ignored. On the contrary, the effects of boundary conditions on flow dynamics in small shallow water bodies has to be accurately accounted for;
2. these models have been mostly developed to study long-term effects of large-scale climate on lakes, which is difficult to do for small lakes due to the spatial resolution used in these models;
3. using these models for small reservoirs requires detailed long-term hydro-climatological field measurements to validate the model results where such data are rarely available for small shallow lakes;
4. one of the main challenges in using these models for small shallow lakes is the complex interaction between the water surface and the atmospheric boundary layer, which is the most important forcing term for vertical mixing and temperature dynamics in the water body;
5. most of these models do not include the effects of temperature on the flow field in the water body. Although some numerical models implement the temperature induced circulation in lakes and oceans, most of these models use the hydrostatic pressure approximation (Hodges et al., 2000; Svensson, 1998). According to some research findings, vertical velocity calculated using the hydrostatic pressure approximation can lead to numerical errors especially for the scalar transport equation in shallow water bodies (Casulli, 1997; 1999; Casulli and Cheng, 1992; Chen, 2003a; 2003b; Chen et al., 2003);
6. in deep lakes, the lake-bed contours have little influence on the overall flow pattern in the water body. However, in small shallow water lakes, lake-bed variations have a stronger influence on the flow patterns due to their proximity to the surface and thus should be considered accurately. Therefore accurate bathymetry of these water bodies should be used in their simulations;
7. in spite of the importance of using real physical boundary conditions in small shallow lake simulations, applying complex and time varying boundary conditions, especially over the water surface, in most of these models is very challenging.

Computational Fluid Dynamics (CFD) simulations are capable of predicting flow dynamics and temperature distributions in reservoirs with a better insight into the main mechanisms leading to stratification and circulation. CFD has widely been used in many environmental and water resources studies and has been considered as an economical and efficient tool in the simulation and analysis of the physics of fluid dynamics (Bartzanas et al., 2013; Chen et al., 2013; Goula et al., 2008; Lee et al., 2013; 2010).

Recently, some well validated commercial CFD codes (e.g. ANSYS Fluent, PHOENICS) and open-source codes (e.g. TELEMAC-MASCARET, Delft3D) have become available (ANSYS, 2016; Deltares, 2016; Open Telemac-Mascaret Consortium, 2016). Several studies have been conducted using these codes to obtain the hydrodynamic characteristics of shallow water bodies (Haque et al., 2007; Politano et al., 2008). Besides some limitations and difficulties in modifying, developing and applying these codes, the small aspect ratio of the computational grid may lead to excessive computational time, instability, and storage requirements in shallow water flow simulations (Lee, 2007).

Considering the limitations of conventional lake models, especially for data scarcity conditions, this study discusses the development of a framework for three-dimensional hydrodynamic and hydrothermal simulation of small shallow inland water bodies to investigate their circulation and temperature dynamics. In comparison with other codes, the model developed in this study can improve implementation of the specific issues relevant to small shallow water bodies which are: 1) produce the bathymetry of the water body applicable in the model by using coarsely measured bathymetric data; 2) generating the computational grid that matches the real geometry and refines the boundaries; 3) develop an unsteady, three-dimensional CFD model capable of predicting the hydrodynamics in the water body considering buoyancy effects on the flow; 4) assign physical and real-time initial and boundary conditions in the model, especially over the water surface; 5) facilitate processing of the model results, e.g. getting the flow variables at specific points, and time series of flow variables. The model developed was applied for a real-world lake and the model results were analyzed to find out the effects of local micrometeorological parameters on flow and temperature dynamics in similar water bodies.

2. Description of small shallow lake framework

Generally, doing a CFD simulation requires the definition of the physical geometry, fluid properties, initial conditions, forcing boundary conditions, and numerical methods for reliable results. In the case of small shallow inland water bodies, CFD simulation requires an additional degree of complexity beyond a typical industrial CFD simulation due to the complexity of the natural processes that drive the system.

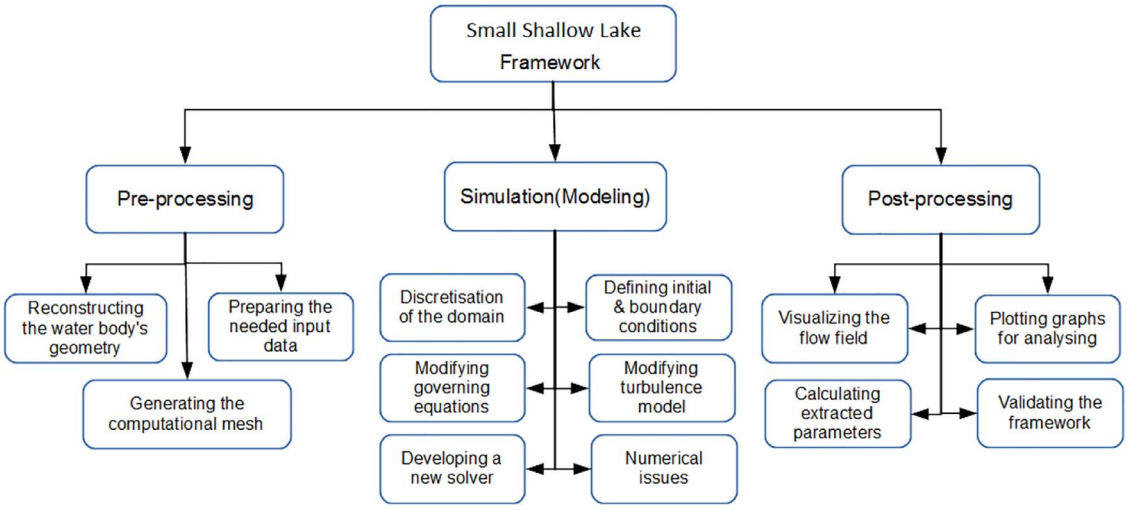

Fig. 1. Components of the proposed framework (Small Shallow Lake Framework) for simulating Small Shallow water bodies.

Most of the driving forces in a small shallow water body simulation such as solar radiation (short-wave radiation), wind speed, precipitation, cloud cover, air temperature and water surface temperature, variation in water composition (such as salinity and density) and the possibility of a stratified flow vary in time and make it difficult to include their effects in the simulation. Finding an appropriate model to compute the heat fluxes through the water surface, the evaporative (latent heat) flux and the source heat due to the penetration of the incident short-wave radiation, comes with a high degree of uncertainty. All of these complexities introduce approximations and subsequent sources of modeling error into the CFD results (Callister, 2008).

Considering these restrictions, a framework is developed in this study to simulate the flow field and heat transfer in small shallow water bodies taking into account the real bathymetry, complex boundary conditions based on available field observations and buoyance effects. This framework is totally based on open-source software and covers all steps needed in the simulation , from generating the geometry of the lake to visualizing the results of the simulation.

The framework consists of three main components depicted in Fig. 1. Since the main goal of the study is to develop a model based on open-source toolboxes, all software used are open-source and allow continuous community-based improvement of the model without any requirement for software licenses. The main toolkit used is *OpenFOAM*, a powerful CFD simulation toolkit, which uses the finite volume numerical schemes to solve the governing equations (OpenFOAM, 2016). OpenFOAM has the required modifications implemented in its standard built-in components, e.g. modified turbulence model, complex boundary condition, etc. All these changes have been tested and debugged and therefore, this framework can be applied to similar water bodies with no need for debugging.

3. Pre-processing phase

The pre-processing stage which is the first step in the framework, as shown in Fig. 1, has two main issues that should be addressed. The first one is preparing the input files needed by the model to read constant, time-dependent parameters, such as measured values for water surface temperature, short-wave radiation, relative humidity, wind speed, etc. All model input parameters are prepared by a home-made code using *python*. This code reads the measured values, analyses and validates them and checks the quality of the input data (i.e. quality control of measured micrometeorological data by some criteria such as sensor range, climate range, temporal step, temporal delta, temporal sigma, spatial interpolation, and using external available data) before making it readable in the CFD simulation(e.g. using in grid generation or modeling by *OpenFOAM*). The generated input files are then used in the model as the time varying boundary conditions or as time-dependent source/sink terms in the turbulence model and flow equations (Section 4.2 and Section 4.4.1). The second issue which should be dealt with in this phase is the generation of the computational grid which is described in more detail in Section 3.2. The general overview of pre-processing phase tasks are illustrated in Fig. 2.

3.1. Reconstructing the water body's geometry

In most small and shallow inland water bodies there are no high-quality measurements of the bathymetry or sufficient data to build the geometry of the computational domain needed in CFD modeling. This could be as a result of logistical difficulties or due to the high cost of doing measurements over these water surfaces. Most available tools and software used to generate the water surface fail mainly due to the small ratio of the vertical to the horizontal dimensions, H/L where H is the depth and L is the horizontal length. For instance, for the investigated lakes in the current study, this ratio, H/L, varies from 0.0002 to 0.004. The initial measured bathymetry is a point-cloud which contains a set of $x-$,$y-$ and $z-$coordinates of measured points (the bathymetric measurement is described in Section 7.1). Using this coarse point-cloud, the generated surfaces were very poor and not applicable in the model. To resolve this problem, a robust, straightforward and generalizable approach was developed in this framework to reconstruct the water surface, bottom and side surfaces of the water body using the coarsely measured bathymetry depicted in Fig. 3(a) through Fig. 3(e). Using the open-source tools mentioned previously in Fig. 2, the initial point-cloud was improved to generate acceptable surfaces for CFD simulations. Reconstructing the surfaces of inland water bodies includes the following steps.

1. Reading the initial measured bathymetric data which contains the $x-$,$y-$ and $z-$coordinates of measured points at the bottom and sides of the lake, separated with a tab, called initial point-cloud. For example, for lake Winkogo, the initial point-cloud consists of 1,838 points. This initial point-cloud has some problems generating an applicable geometry for using in the CFD simulations because, first, this point-cloud does not have adequate resolution. In some regions there is no point to generate the surface at all. Second, it has no point sets to define the water surface boundary. The measured points with highest elevation (or $z-$values) do not represent the water surface however it is important to define this boundary in the point cloud. Third, there are some points in the point-cloud that do not belong to the lake bathymetry. It means that the points over the

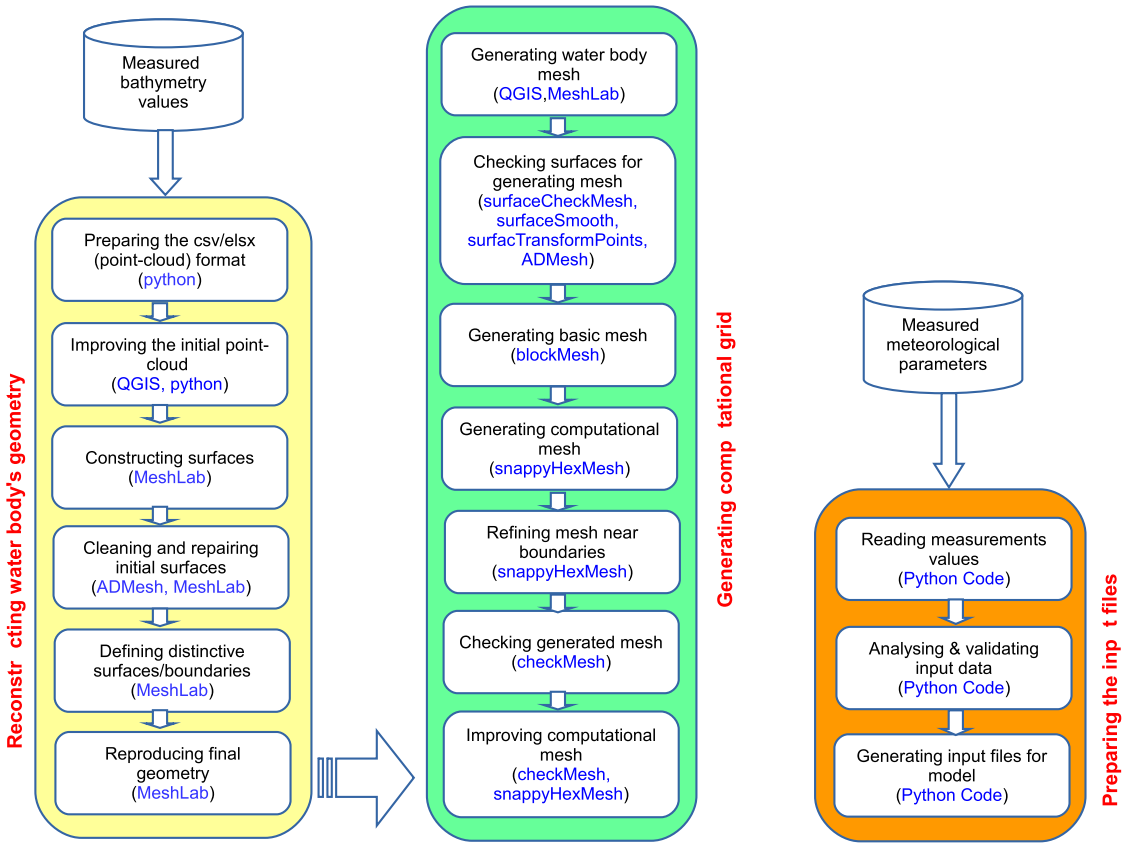

Fig. 2. The details of pre-processing phase of the proposed framework. The tools and software used are presented in the parentheses.

dry areas in the shoreline should not be included in the geometry of water body, and therefore, should be removed from the point-cloud. Fourth, the vertical scale compared with the horizontal lengths is very small (around 2: 1000) and causes significant errors in generating the geometry. Fifth, the point samples are not uniformly distributed over the model surface (Fig. 3(a)).

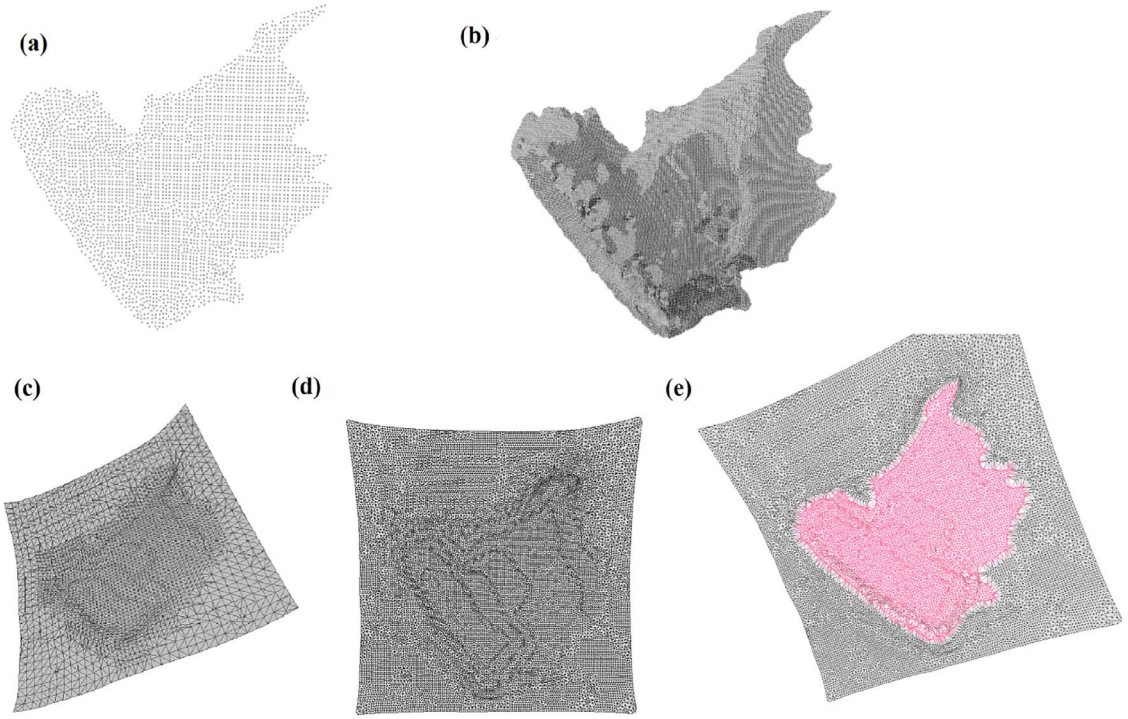

Fig. 3. Chained processes of generating surfaces (in STL format) from an initial point-cloud in lake Winkogo: **(a)** The plan view of initial point-cloud; **(b)** the improved point-cloud using proposed approach to generate the water body's geometry; **(c)** initial generated surface; **(d)** refining and reconstructing the initial generated surface; and **(e)** separating the surfaces and removing unneeded parts.

2. Improving the initial point-cloud with some extra points using the interpolation methods from *QGIS* (Open Source Geographic Information System) (QGIS, 2016). In the case of lake Winkogo, the improved point-cloud contains 42,412 points which could be sufficient to produce smooth surfaces (Fig. 3(b)).
3. Generating a text file, preferably in *csv* format containing the points' coordinates interpretable by *MeshLab*, an open-source and extensible toolkit for generating, editing and processing unstructured 3-D triangular meshes, to generate the surfaces of the water body (MeshLab, 2016).
4. Reading the improved point-cloud, checking, modifying and generating an *STL* (STereoLithography/Standard Triangle Language) file by using *MeshLab* which could be handled by mesh generator toolboxes. In an *STL* file, multiple objects can be represented as a list of triangles that conform to their surfaces. It should be noted that, in this step, the normal vectors of point-sets and the quality of generated surfaces should be checked. Due to the very small ratio of the depth to the horizontal dimensions, prior to generating the *STL* file, the dimensions should be scaled up in $z-$direction (depth) to generate an acceptable surface. The method used to develop an applicable surface from the improved point-cloud should be able to infer the topology of the surfaces, accurately fit the noisy data, and fill holes reasonably. It was found that the "Poisson" method was befitting for reconstructing the surface from the point-cloud. Poisson Surface Reconstruction is one of the approaches used to obtain a smooth and watertight surface (Fig. 3(c) through Fig. 3(e)). As a final task, it is suggested to do some repairing and cleaning processes (such as merging close vertices, removing duplicate faces, removing duplicate vertex, etc.). The final generated surfaces for lake Winkogo are depicted in Fig. 4(a) and (b).
5. To be able to assign the right boundary conditions to the surfaces in the model, distinctive surfaces should be defined in the reconstructed *STL* file. In most inland water body models, there are mainly two different surfaces: a) a surface that represents the water surface; and b) a surface that represents the bottom and sides. Defining extra surfaces such as inlet and outlet boundaries could be done easily in the proposed approach.

3.2. Generating the computational grid

The next step is to translate the physical domain into a numerical domain, or computational mesh. The generated mesh has to accurately represent the shape of the water body. The quality of the computational grid has a clear impact on the accuracy of the CFD simulations and influences significantly the convergence speed of the simulation. In spite of the importance of the computational grid in CFD simulations, generating an appropriate high quality grid (i.e. low skewness, low orthogonality, aspect ratio near 1.00, etc.) remains a big challenge, while using inappropriate grids will lead to large errors.

The proposed framework uses a right hand coordinate system, with the $z-$axis positive in the upward direction, normal to the water surface, and $z = z_{ws}$ represents the maximum depth of lake, corresponding to the water surface. The origin is located in the lower left-hand corner of the mesh, when viewed in the $xy-$plane. Keeping with this convention, the $x-$axis is aligned to be positive in the easterly direction, with the $y-$axis positive in the north direction.

Horizontal grids are generated depending on the geometrical boundaries conforming to improved measured bathymetry. Fig. 4(c) and (d) show details of the generated grid in lake Winkogo. The typical cell size in the lake is 10 m and 0.1 m in the horizontal and vertical directions respectively. Near the free water surface, refining the grid is essential especially in vertical direction (cell heights are about 0.01 ~ 0.02 m) to capture the strong temperature and velocity gradients which exist at the air-water interface (Haque et al., 2007).

In generating the computational grids there is always a trade-off between running time and good results. This results in high aspect

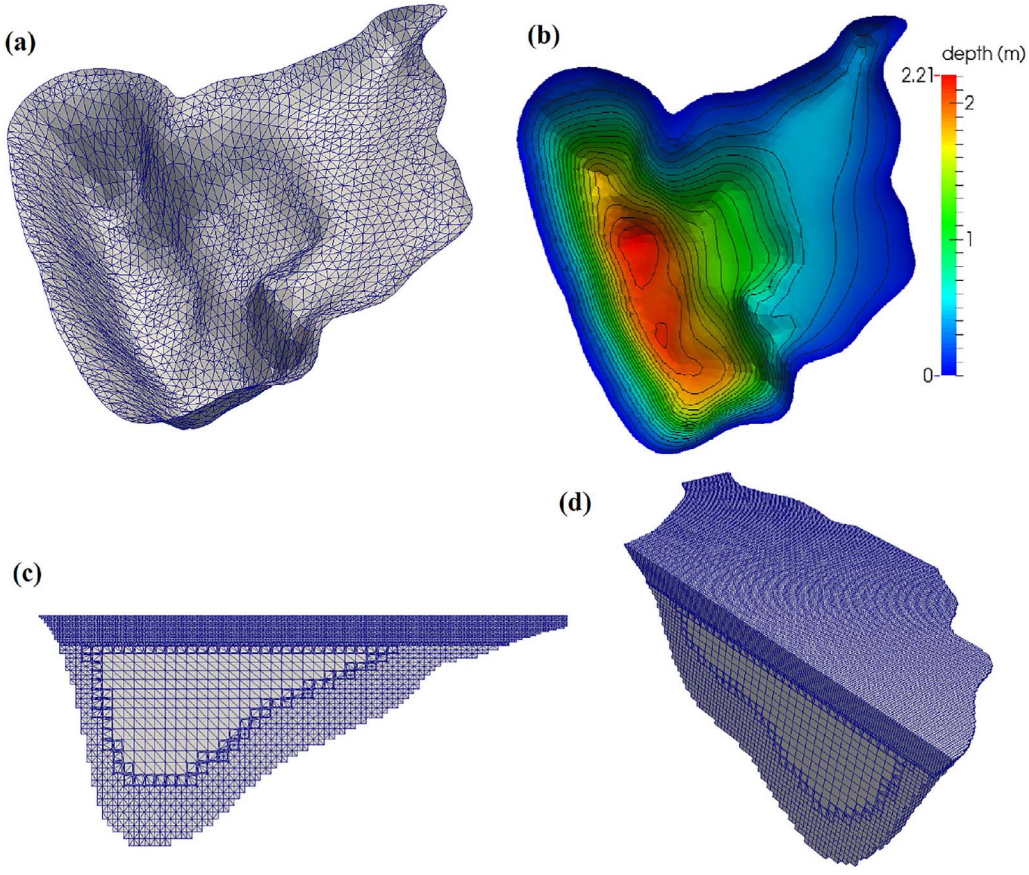

Fig. 4. (a) Example of the final generated surface (in STL format) of a water body (lake Winkogo) which is used in generating computational mesh; **(b)** 3-D view of water body's geometry and the depth contours; **(c)** the vertical section of the generated computational grid of the water body; and **(d)** 3-D view of the computational grids (vertical dimension is exaggerated by 50).

ratios and long flat cells. Generally, generating computational grids for non-uniform geometries, in which one of the directions is much smaller than the others, seems problematic for most available grid generators. This problem can be resolved by scaling/rescaling the dimensions in the desired direction (Brockhaus, 2011). It is strongly suggested that the adequacy of the grids is investigated by comparing the results of the model with different mesh sizes. The use of fine mesh in simulations often produces better agreement in some regions of studied domain, although it needs more computational resources and more running time.

The grid generation is done with an *OpenFOAM*-utility *snappyHexMesh (sHM)* (snappyHexMesh, 2016). Unlike most commercial and automatic grid generators *sHM* is a script-driven tool used to generate unstructured computational grids containing hexaedra and split-hexaedra meshes (Brockhaus, 2011). *sHM* proved to be very flexible with different domain configurations. *sHM* allows one to use *STL* files which represent the domains' topography in complex geometries.

In general, the process of generating computational grids for small shallow lakes includes the following steps.

1. Checking the quality of reconstructed surfaces (*STL* file) and cleaning or repairing the surfaces which involves: a) checking the surface by using *surfaceCheck* utility (*OpenFOAM*); b) smoothing the surfaces by using *surfaceSmooth* utility; c) rotating the surface to decrease the non-orthogonality of the generated mesh by using *surfaceTransformPoints* utility; and finally, d) cleaning and repairing the final surface by using *ADMesh*, a program for processing triangulated solid meshes(ADMesh, 2016). The final cleaned, repaired and improved surface can be used to generate the computational grids.
2. Generating a background block structured mesh which contains the outlines of the computational domain. The quality of the mesh is significantly affected by the aspect ratio, fineness, orientation and other properties of the initial mesh used.
3. Generating the computational grid using the *snappyHexMesh (sHM)* utility. *sHM* uses a non-interactive approach to generate the grid hence could be considered as an almost ideal tool for automating mesh generation (Brockhaus, 2011). Notwithstanding this advantage, it must be noted that this tool does not have a graphical interface so controlled from its dictionary by commands.
4. Refining the mesh near the boundaries to resolve high gradients in flow parameters using the available options in *sHM*.
5. Checking the quality (maximum aspect ratio, non-orthogonality, skewness, etc.) of the generated mesh by using *checkMesh* utility and improving the grids if necessary.

4. Simulation phase

4.1. Governing equations

The flow field in morphometrically complex small shallow water bodies is governed by the conservation laws of mass, momentum and internal energy. Combining the flow simulation and heat transfer in the water body alongside the complex geometry of lake introduces extra complexities to the model. In water bodies, the wind shear stress due to air flow and changes in water density due to temperature evolution are considered as driving forces. Even though the thermodynamic properties of water are assumed to be constant, the buoyancy body force term in the momentum equation is added allowing one to relate density changes to temperature. The flow is assumed to be three-dimensional, incompressible Newtonian fluid using Boussinesq approach (Tritton, 2007; Tsanis, 2006). Based on these assumptions the Reynolds Averaged Navier Stokes (RANS) equations are written as (Ferziger and Perić, 2002; Massel, 1999; White, 1991):

$$\frac{\partial u_j}{\partial x_j} = 0 \tag{1}$$

$$\frac{\partial u_i}{\partial t} + \frac{\partial}{\partial x_j}(u_j u_i) - \frac{\partial}{\partial x_j}\left\{\nu_{eff}\left[\left(\frac{\partial u_i}{\partial x_j} + \frac{\partial u_j}{\partial x_i}\right) - \frac{2}{3}\left(\frac{\partial u_k}{\partial x_k}\right)\delta_{ij}\right]\right\} = -\frac{1}{\rho_k}\frac{\partial p}{\partial x_i} + g_i[1 - \beta(T - T_{ref})] \tag{2}$$

$$\frac{\partial T}{\partial t} + \frac{\partial}{\partial x_j}(Tu_j) - \alpha_{eff}\frac{\partial}{\partial x_k}\left(\frac{\partial T}{\partial x_k}\right) = S_T(t, x_k) \tag{3}$$

where u_i is the velocity component in x_i direction (ms), t is time (s), p pressure (Pa), T temperature (K), $\nu_{eff} = \nu_0 + \nu_t$ is the effective kinematic viscosity (m^2s^{-1}), with ν_0 and ν_t denoting molecular and turbulent viscosity, respectively, g_i the gravity acceleration vector (ms^{-2}), T_{ref} a reference temperature (K), β the coefficient of expansion with temperature of the fluid (J $kg^{-1}K^{-1}$) and δ is the delta of Kronecker (dimensionless), ρ_k the effective (driving) kinematic density (dimensionless), α_{eff} heat transfer conductivity (m^2s^{-1}) and S_T is the heat source term (Ks^{-1}) in the lake due to the penetrated solar radiation. The Boussinesq approximation is valid under the assumption that the density differences are sufficiently small to be neglected, except where they appear in the term multiplied by g_i (Corzo et al., 2011; Fredriksson, 2011). According to White (1991) and Ferziger and Perić (2002), the Boussinesq approximation introduces errors less than 1% for temperature variations of 2 K for water or 15 K for air. In the model, for incompressible flows the water density is computed as a linear function of temperature as

$$\rho_k = 1 - \beta(T - T_{ref}) \tag{4}$$

$$\rho = \rho_k \times \rho_0 \tag{5}$$

where ρ is the temperature dependent density (kgm^{-3}), and ρ_0 is water density at reference temperature (kgm^{-3}). Heat transfer conductivity in water body is given by:

$$\alpha_{eff} = \alpha_t + \alpha_0 = \frac{\nu_t}{Pr_t} + \frac{\nu_0}{Pr} \tag{6}$$

where α_{eff} is the effective kinematic viscosity (m^2s^{-1}), α_0 and α_t denote molecular and turbulent heat transfer conductivity, respectively, ν_0 molecular kinematic viscosity (m^2s^{-1}), ν_t turbulent kinematic viscosity (m^2s^{-1}), Pr is Prandtl number (a dimensionless number defined as the ratio of momentum diffusivity to thermal diffusivity which controls the relative thickness of the momentum and thermal boundary layers), and Pr_t turbulent Prandtl number (unitless). Changes in temperature in water bodies might occur mainly due to the heat exchange across the air-water interface. Accurate estimation of the heat fluxes is required in the simulation of temperature dynamics in the water body (Politano et al., 2008). Atmospheric heat fluxes include incoming short-wave (solar) and long-wave (atmosphere) radiations, outgoing long-wave radiation, conductive heat at the free surface and evaporative heat flux. Computationally, all of the heat flux components except for incoming short-wave radiation are considered as boundary condition at the water surface.

Adding the incoming short-wave radiation in the temperature source term (S_T) allows the radiation to penetrate and be absorbed through a specific depth of the water column rather than only at the air-water interface (Losordo and Piedrahita, 1991; Wood et al., 2008). The heat source term using Lambert-Beer low is written as:

$$S_T(z^*, t) = \frac{1}{\rho_0 C_p}\frac{\partial Q_{Rs}^{z^*}}{\partial z} \tag{7}$$

$$Q_{Rs}^{z^*} = Q_{Rs}^0 \sum_{i=1}^{7} f_i \exp(-\eta_i z^*) \tag{8}$$

Table 1
Short-wave radiation bandwidth fractions of the total energy (f) and composite attenuation coefficients (η) (adopted from Branco and Torgersen, 2009).

Wavelength(nm)	f	$\eta(m^{-1})$
< 400 (UV)	0.046	Assume same as VIS (i.e. 400–700 nm)
400–700 (VIS)	0.430	Obtained from measurements (here assumed 3.00)
700–910	0.214	2.92
910–950	0.020	20.40
950–1090	0.089	29.50
1090–1350	0.092	98.40
> 1350	0.109	2880.00

$$S_T(z^*, t) = \frac{Q^0_{Rs}}{\rho_0 C_p} \sum_{i=1}^{7} \eta_i f_i \exp(-\eta_i z^*) \tag{9}$$

where z^* is downward vertical distance from the water surface (m), C_p specific heat of lake water (J kg^{-1}K^{-1}), $Q^{z^*}_{Rs}$ is heat flux due to penetrated solar radiation at a depth z^* within the water (Wm^{-2}), Q^0_{Rs} is the net solar radiation at the air-water interface (Wm^{-2}), f_i is the fraction of energy contained in the ith bandwidth (dimensionless), and η_i is the composite attenuation coefficient of the ith bandwidth (m^{-1}) (Branco and Torgersen, 2009; Momii and Ito, 2008). The values of f_i and η_i are presented in Table 1. The attenuation coefficient (light extinction coefficient) for visible light theoretically is a function of wave length, temperature and water turbidity and typically ranges from 0.02 to 31.60 for inland shallow waters (Bigham Stephens et al., 2015; Goudsmit et al., 2002; Losordo and Piedrahita, 1991; Politano et al., 2008; Smith and Baker, 1981). In inland water bodies, usually the extinction coefficient is computed by using a linear function of the Secchi depth (Idso and Gilbert, 1974; Politano et al., 2008). According to Henderson-Sellers (1984), the value of η is largely affected by water turbidity and macrophyte population in the water body. Based on measured Secchi disc depth, Williams et al. (1981) suggested that, under non-eutrophic conditions, η can be represented by:

$$\eta = 1.1 \times d_s^{-0.73} \tag{10}$$

where d_s is the Secchi disc depth (m). To calculate η accurately, detailed measurements of macrophyte population are necessary, which are not normally available. For this study, the attenuation coefficient was assumed to be $\eta = 3.0$ m^{-1}.

The net solar radiation at the air-water interface (Q^0_{Rs}) is given by the following equation (Subin et al., 2012):

$$Q^0_{Rs} = (1 - r_{ws})R_s \tag{11}$$

where R_s is the incoming short-wave radiation at the water surface (Wm^{-2}) and r_{ws} is the reflection coefficient of solar radiation from water surface (dimensionless). The incoming short-wave radiation (R_s) can be easily measured over the water surface or even on the dry areas surrounding lake. An alternative way, but with more uncertainty, is using an experimental equation presented in the literature (e.g. Gianniou and Antonopoulos, 2007). The incoming short-wave radiation over the water surface depends on cloud cover and this should be taken into account in calculating this parameter.

4.2. Turbulence model

In order to model the turbulent flows using the RANS approach requires a turbulence model to compute the Reynolds stresses and close the system of mean flow equations. According to the number of additional transport equations which should be solved along with the RANS equations, a wide range of turbulence models has been proposed (e.g. zero, one, two or seven equation models).

Although the turbulence model can affect the water and heat flow in small shallow water bodies, the investigation of the turbulence models is not the main aim of this study. In simulating water flow alongside heat transfer in inland water bodies, it was found that the implemented realizable $k-\varepsilon$ model provides better results than other $k-\varepsilon$ models (Shih et al., 1995; Wang, 2013). In this model, dissipation rate of fluctuations is approximated by the dynamic vorticity equation. In addition, the realizable $k-\varepsilon$ has been shown to enhance the numerical stability in turbulent flow simulations (Shih et al., 1995). In this model, the turbulent kinetic energy (k in m^{2}s^{-2}) and the dissipation rate of turbulent kinematic energy (ε in m^{2}s^{-3}) were obtained from:

$$\frac{\partial k}{\partial t} + u_j \frac{\partial k}{\partial x_j} = \frac{\partial}{\partial x_j}\left[\left(\nu + \frac{\nu_T}{\sigma_k}\right)\frac{\partial k}{\partial x_j}\right] + \nu_T\left(\frac{\partial u_i}{\partial x_j} + \frac{\partial u_j}{\partial x_i}\right)\frac{\partial u_i}{\partial x_j} - \varepsilon + G_k + G_b + S_k \tag{12}$$

$$\frac{\partial \varepsilon}{\partial t} + u_j \frac{\partial \varepsilon}{\partial x_j} = \frac{\partial}{\partial x_j}\left(\frac{\nu_T}{\sigma_\varepsilon}\frac{\partial \varepsilon}{\partial x_j}\right) + C_1 S\varepsilon - C_{\varepsilon 2}\frac{\varepsilon^2}{k + \sqrt{\nu\varepsilon}} + C_{\varepsilon 1}C_{\varepsilon 3}\frac{\varepsilon}{k}G_b + S_\varepsilon \tag{13}$$

where ν_0 is the kinematic viscosity (m^{2}s^{-1}), ν_t is the turbulent kinematic viscosity (m^{2}s^{-1}), G_k is the production of turbulent kinetic energy by the mean velocity gradient (m^{2}s^{-3}), G_b is the production of turbulent kinetic energy by the buoyancy (m^{2}s^{-3}), S_k (m^{2}s^{-3}) and S_ε (m^{2}s^{-4}) are the source/sink terms which include the effects of wind on k and ε equations respectively. More details about the realizable $k-\varepsilon$ (RKE) model and its terms are presented in Appendix A. When a temperature gradient and a non-zero gravity field are present simultaneously, the k and ε equations include the generation of turbulent kinetic energy due to buoyancy (G_b in Eq. (12)), and the corresponding contribution to the production of ε (G_b in Eq. (13)). The buoyancy-induced turbulence is given by

$$G_b = \beta g_i \frac{\nu_t}{Pr_t}\left(\frac{\partial T}{\partial x_i}\right) \tag{14}$$

where g_i is the component of the gravitational vector in the ith direction and Pr_t is the turbulent Prandtl number. The default value of Pr_t for water used in the standard and realizable $k-\varepsilon$ models is 0.85 (Fluent, 2006; Wang, 2013). In unstable stratification, $G_b > 0$ and turbulence kinetic energy tends to be higher. For stable stratification, $G_b < 0$, the buoyancy force tends to disrupt the turbulence. While the effects of buoyancy on the generation of k are relatively well understood and are commonly included in the turbulence models, the buoyancy effect on ε is less clear (Fluent, 2006). However in the current model, the buoyancy effects on ε are given by Eq. (A.13) which is used in the transport equation for ε (Eq. (13)). The degree to which ε is influenced by the buoyancy is estimated by the non-constant parameter $C_{3\varepsilon}$ (Appendix A).

Standard values of the model constants of the realizable $k-\varepsilon$ turbulence approach in the model equations are (Shih et al., 1995):

$$C_\mu = 0.09;\ C_{\varepsilon 1} = 1.44;\ C_{\varepsilon 2} = 1.92;\ \sigma_k = 1.0;\ \sigma_\varepsilon = 1.3;\ A_0 = 4.0; \tag{15}$$

Depending on the approach used, the effects of wind velocity over the water surface in the model (Sections 4.2.2 and 4.2.1), the source/sink terms (in Eqs. (12) and (13)) can be determined.

4.2.1. Wind effects included as source/sink terms in turbulence model

In small shallow inland water bodies, turbulence produced by wind can be critical. The momentum input at the water surface can be caused by water surface (skin) friction, wave-induced pressure fluctuations and wave and drift-related current interactions (Wang, 2013). Below the wave-affected surface layer, the vertical profiles of the horizontal velocity follow the law-of-the-wall. The classical logarithmic-layer characteristic is thus applicable (Craig and Banner, 1994). The effects of wind speed on the water body can be considered as source/sink terms in the turbulence model's equations (Wang, 2013; Wüest and Lorke, 2003). In this approach the effects of wind shear stress over the flow is implemented in the turbulence equations using source/sink terms (S_k

and S_ε). Using this method, the water surface is modeled using the rigid-lid approach. In this approximation, free surface deformations are ignored (Tsanis, 2006). Assuming a flat surface with zero shear stress, a slip boundary condition (normal component of velocity, u_z, is zero and tangential components, u_x and u_y, are zero gradient) is used for velocity on the water surface boundary:

$$u_x \neq 0; \qquad \frac{\partial u_x}{\partial z} = 0 \tag{16}$$

$$u_y \neq 0; \qquad \frac{\partial u_y}{\partial z} = 0 \tag{17}$$

$$u_z = 0 \tag{18}$$

and the effects of wind stress on k and ε can be parameterized as source/sink terms in Eqs. (12) and (13) as (Wüest and Lorke, 2003)

$$S_k = \frac{u_*^3}{\kappa z^*} \tag{19}$$

$$S_\varepsilon = C_{1\varepsilon}\frac{\varepsilon}{k}S_k \tag{20}$$

It means that the vertical velocity profile near the water surface following the law of the wall and the usual logarithmic function can be applied (Craig and Banner, 1994). In these equations, κ is the von Karman constant (dimensionless), z^* is the vertical distance from the free surface (m), u_* is the friction velocity (ms^{-1}) given by

$$u_* = \sqrt{\frac{\tau_0}{\rho_a}} \tag{21}$$

and the wind stress (τ_0 in kg m^{-1} s^{-2}) can be parameterized as follows:

$$\tau_0 = \rho_a C_D U_{10}^2 = \rho_a u_*^2 \tag{22}$$

where ρ_a is the air density (kg m^{-3}), C_D is the empirical dimensionless drag coefficient (unitless) which mainly depends on wind speed and water surface waves, and U_{10} is the mean wind speed at 10.0 m height (ms^{-1}). For strong winds ($U_{10} > 5$ ms^{-1}) a relationship between C_D and U_{10} is given by a variation of Charnock's law (Charnock, 1955; Markfort et al., 2010; Wüest and Lorke, 2003):

$$C_{D,10} = \left[\kappa^{-1}\ln\left(\frac{10g}{C_{D,10}U_{10}^2}\right) + 11.3\right]^{-2} \tag{23}$$

where g is the gravitational acceleration (ms^{-2}), U_{10} is the mean velocity at a height of 10.0 m and $C_{D,\ 10}$ is surface drag coefficient at a height of 10.0 m above the water surface. The implicit function presented in Eq. (23) converges quickly after a few iterations (Wüest and Lorke, 2003).

In small shallow lakes, wind speed is typically low (commonly $U_{10} < 5$ ms^{-1}) and measurements of the drag coefficient are relatively scarce. Confusingly, in literature the values of $C_{D,\ 10}$ vary over a wide range and are associated with large scatter (Falconer et al., 1991; Goudsmit et al., 2002; Wüest and Lorke, 2003). For this study, the following empirical relationship for low wind speeds is used (Markfort et al., 2010; Wüest and Lorke, 2003):

$$C_{D,10} = 0.0044 \times U_{10}^{-1.15} \tag{24}$$

In this equation, the wind velocity at height of 10.0 m above the water surface (U_{10}) is needed. If the wind velocity measurements are available in height z, the following equation can be used to estimate the wind velocity at height of 10.0 m above the water surface (U_{10}) (Schertzer et al., 2003; Verburg and Antenucci, 2010):

$$U_{10} = U_z\left(\frac{10}{z}\right)^{1/7} \tag{25}$$

In small inland water bodies such as the one studied, the wave field is typically not fully developed due to the small fetches and, consequently, the wind-induced turbulence obtained from Eq. (19) through Eq. (24) will be underestimated. As the original built-in turbulence model in *OpemFOAM* does not include these terms, they have to be added to k and ε equations as shown in Eqs. (12) and (13) which could introduce more complexity to the model. Assuming constant wind speed values and using this approach is straightforward to do and will require less run time (Wang, 2013). The most noticeable advantage of this approach is simplifying the assigned velocity boundary condition over the water surface.

4.2.2. Wind effects considered as boundary condition

As stated in Section 4.2.1 it is possible to consider the effects of wind velocity as source/sink terms in the k and ε equations in the turbulence model. The second and most common approach is considering the wind effects as a boundary condition over the water surface (Section 4.4.1). In this situation the source/sink terms (S_k and S_ε in Eqs. (12) and (13), respectively) are eliminated from the turbulence model equations:

$$S_k = 0; \qquad S_\varepsilon = 0 \tag{26}$$

4.3. Initial conditions

In most small and shallow lakes simulations it is assumed that at $t = 0$ (initial condition), the water is at rest with a given temperature distribution, homogeneous or stratified. Although the initial values of flow parameters have no effect on the results, assigning the real initial conditions in the model could accelerate the convergence of numerical computations. As for most reservoirs there is often no sufficient data to generate the initial distribution of temperature and velocity, the measured temperature profile at the start of simulation (T at $t = 0$) throughout the entire lake could be used as initial condition. For the velocity, it is assumed that there is no current and zero flow is assumed. If measurements are available for other parameters in the water body, they could be easily applied as initial conditions in the model. The initial conditions are set by using *funkySetField*, a tool available in *swak4Foam* libraries (Gschaider, 2016), with python-based functions applicable within the *OpenFOAM* platform. To prevent numerical instabilities in the model, a weak (non-zero value) initial turbulence is assumed in the simulation (Verdier-Bonnet et al., 1999).

4.4. Boundary conditions

In the CFD simulation of small shallow inland water bodies, assigning the correct conditions on the boundaries is important and the results of the simulation can be directly affected by them (Elo, 2007). The boundary conditions in the lake models are time varying and complicated. Water surface temperature and circulation in the water body are strongly influenced by time varying micro-meteorological conditions. Depending on the available data, different types of boundary conditions can be used for the reservoirs in the current framework.

4.4.1. Free water surface boundary conditions

Generally, in water bodies, physical and chemical properties (such as kinetic energy, momentum, heat, etc.) exchanges occur in the surface boundary layer (SBL) which is mostly driven by wind- and heat flux-induced turbulence. Therefore, assigning correct boundary conditions on the water surface is a fundamental step in simulating the flow in lakes (Craig and Banner, 1994; Etemad-Shahidi et al., 2010).

4.4.2. Velocity boundary condition

Wind is one of the most important forces that drive free surface movement. Wind affects lake currents, sensible and latent heat fluxes and turbulence as well as surface waves. The wind drag coefficient is significantly affected by the water surface wave development. Waves produce additional roughness and consequently increase the friction at

the free water surface. This mechanism enhances transferring momentum flux from air to water (Wang, 2013). Circulation in the lake is mainly driven by wind shear on the water surface (Liu et al., 2012). The wind-induced circulation significantly affects the dynamics of water temperature and consequently water quality and ecosystem in the inland shallow water bodies. The generated circulation in the water body is very complicated and this study is far from solving all details. It is assumed that wind induced circulation in a closed basin occurs when stresses due to winds are applied at the free surface as a boundary condition. The exchanged momentum from atmospheric boundary layer to the water surface by the wind blowing across the water surface has typically been modeled using a stress boundary condition, which is a function of the viscosity (ν). In this study, the effects of wind shear stress over the flow is considered through two approaches which use different boundary conditions for velocity (U) on the water surface:

I) Shear Stress over the Water Surface: in this approach the effects of wind shear stress over the flow was considered as time-dependent shear stress boundary condition over the water surface and given by

$$\left[\nu_{eff}\frac{\partial u}{\partial z}\right] = \frac{\tau_{sx}}{\rho_0} \tag{27}$$

$$\left[\nu_{eff}\frac{\partial v}{\partial z}\right] = \frac{\tau_{sy}}{\rho_0} \tag{28}$$

where

$$\tau_{sx} = \rho_a C_D u_w \sqrt{u_w^2 + v_w^2} \tag{29}$$

$$\tau_{sy} = \rho_a C_D v_w \sqrt{u_w^2 + v_w^2} \tag{30}$$

τ_{sx} and τ_{sy} are horizontal shear stress components over the water surface (kg $m^{-1}s^{-2}$), u_w and v_w are horizontal components of the mean wind speed over the water surface (ms^{-1}), and ν_{eff} is the effective kinematic viscosity (m^2s^{-1}), ρ_a is the air density (kg m^{-3}), ρ_0 is the water density (kg m^{-3}), and C_D (dimensionless) is the empirical dimensionless drag coefficient calculated using Eq. (24). The normal component of velocity over the water surface boundary is calculated by:

$$u_z = 0 \tag{31}$$

Therefore on the water surface the following conditions are applied as velocity boundary condition:

$$\frac{\partial u_x}{\partial z} = \frac{C_D \times \rho_a \times |U|}{\rho_0 \times (\nu_0 + \nu_t)} \times u_x \tag{32}$$

$$\frac{\partial u_y}{\partial z} = \frac{C_D \times \rho_a \times |U|}{\rho_0 \times (\nu_0 + \nu_t)} \times u_y \tag{33}$$

$$u_z = 0 \tag{34}$$

where all terms used here are defined in the previous equations. Without the wind shear stresses, Eqs. (32) and (33) lead to no flux conditions along the water surface boundary.

II) Sink/Source Terms in Turbulence Equations: as described in Section 4.2.1, for this type of boundary condition the effects of wind speed are implemented in the turbulence equations and a slip condition is assumed for velocity. For a scalar, it can be replaced by a zero-gradient condition and for a vector it is equal to zero fixed value and zero fixed gradient for the normal and tangential components respectively. This approach is suggested for high wind speeds or approximately uniform wind speeds.

4.4.3. Turbulence boundary conditions

At large scales, it is generally assumed that wind creates a boundary-layer close to the upper surface where a constant shear stress is assumed and consequently the vertical velocity profile follows the law-of-the-wall (Craig and Banner, 1994; Verdier-Bonnet et al., 1999). The production of turbulent kinetic energy in this logarithmic region can be computed by the wind-induced vertical gradient of energy flux. In this study, the effects of wind surface waves in turbulence was ignored due to low wind speeds hence the standard wall functions were applied to the turbulent parameters k and ε on the water surface boundary. More details on using wall functions and their limitations in turbulence models, such as the near boundary grid size, can be found in Abbasi et al. (2016b).

4.4.4. Temperature boundary conditions

The proposed framework is flexible in working with different temperature boundary conditions on the water surface. The type of boundary for temperature on the free surface depends on the available parameters:

I) Using Measured Water Surface Temperature as Boundary Condition: if the measured water surface temperature values are available this type of boundary condition can be applied on the free water surface (Dirichlet type):

$$T(t) = T_m(t) \tag{35}$$

where $T_m(t)$ is the measured water surface temperature varying with time. This type of boundary condition is less practical in small shallow water bodies simulations due to the requirement for additional measurements of temperature over the water surface which are rarely available for most small shallow lakes. However, the big advantage of using this boundary condition is the avoidance of uncertainties in computing the heat flux components over the water surface (Goudsmit et al., 2002).

II) Heat Fluxes as Boundary Condition: heat exchanges across the air-water interface which consist of long-wave and short-wave radiations, sensible and latent heat fluxes, impact the temperature changes in the water body. Although precise estimation of the heat flux components is important in the simulation of flow dynamics in a water body, the parameterization of these terms is complex and contains a large amount of uncertainties because they are controlled mainly by time varying micrometeorological conditions. In this study, the heat flux over the water surface was divided into two categories: a) non-penetrative radiations which include sensible heat and latent heat fluxes and long-wave radiation, which affect only the water surface and are considered as surface heat fluxes; b) penetrative radiation which contains short-wave radiation that can penetrate through the water column after passing through the water surface. To take into account the distributed heat due to this heat flux, it is not included in the boundary condition. Rather, this flux is considered as a heat source in the water body as shown in Eq. (3).

At the water surface, the net surface heat flux (H_{net} in Wm^{-2}) which diffused away from the lake surface is expressed by the following equation (Neumann boundary condition) (Goudsmit et al., 2002):

$$\rho_0 C_p\left(\alpha_{eff}\frac{\partial T}{\partial z}\right) = H_{net} \Rightarrow \frac{\partial T}{\partial z} = \frac{H_{net}}{\rho_w C_p \alpha_{eff}} \tag{36}$$

The net heat transfer across the air-water interface includes four heat flux terms (Ahsan and Blumberg, 1999; Goudsmit et al., 2002):

$$H_{net} = H_{LA} - H_{LW} - H_S - H_E \tag{37}$$

where H_{LA} is the net long-wave (atmospheric) radiation from atmosphere, H_{LW} is the long-wave radiation from the water surface, H_S and H_E are the sensible and latent heat fluxes between the lake surface and the atmosphere, respectively (all terms in Wm^{-2}). As all these heat fluxes change over time, they have to be updated at each time step. Out of these heat flux components, only the incoming short-wave radiation was measured and the rest were calculated within the model using standard formulations.

Long-wave radiation: the long-wave radiation is composed of energies emitted from the water surface and absorbed from the atmosphere. Atmospheric long-wave radiation is calculated from the Stefan–Boltzmann law (Ahsan and Blumberg, 1999; Goudsmit et al.,

Table 2
Values of the model constants (water in 20 °C).

Parameter	Definition	Unit	Value
r_a	Reflection coefficient of atmospheric radiation from water surface	[−]	0.03
ε_a	Emissivity of atmosphere	[−]	0.87
ε_{ws}	Emissivity of water surface	[−]	0.97
σ	Stefan–Boltzman constant	[W m $^{-2}$ K^{-1}]	5.669×10^{-8}
P_{atm}	Atmospheric pressure	[Pa]	102′000
ρ_a	Air density	[kg m^{-3}]	1.186
ρ_0	Water density	[kg m^{-3}]	998.2336
Pr	Prandtl number	[–]	7.07
Pr_t	Turbulent Prandtl number	[–]	0.85
κ	von-Karman constant	[–]	0.41
C_p	Specific heat of water	[m^2 s^{-2}K^{-1}]	4.1818×10^3
T_{ref}	Reference temperature	K	293.15
β	Thermal expansion coefficient	K^{-1}	0.207×10^{-3}
ν_0	Molecular viscosity	[m^2 s^{-1}]	1.004×10^{-6}

2002):

$$H_{LA} = (1 - r_a)\,\varepsilon_a \times \sigma\, T_a^4 \tag{38}$$

where H_{LA} is the net long-wave (atmospheric) radiation from the atmosphere per unit surface area (Wm^{-2}), r_a is the reflection coefficient of atmospheric radiation from water surface (unitless), σ is Stefan–Boltzman constant, and T_a is absolute air temperature in K. ε_a is emissivity of atmosphere and usually depends on vapor pressure, air temperature and cloud cover. Although the effects of these parameters on ε_a can be easily implemented in the model, due to small changes its value is assumed constant in this study (Table 2). Similarly, long-wave radiation emits from the water surface estimated by (Ahsan and Blumberg, 1999; Goudsmit et al., 2002; Shufen et al., 2007):

$$H_{LW} = \varepsilon_{ws} \times \sigma T_{ws}^4 \tag{39}$$

where ε_{ws} is the dimensionless emissivity of water whose numerical values vary from 0.96 to 0.97 and T_{ws} is the absolute temperature of water surface in K (Lee, 2007). In Table 2 the values of constant parameters used are presented.

Sensible heat flux: sensible heat flux (H_S) over the water surface associated with the temperature difference between the air and underlying water surface. To estimate this turbulent heat flux, the following equation is used:

$$H_S = h_s(T_{ws} - T_a) \tag{40}$$

where H_S is the convective heat transfer or sensible heat flux in Wm^{-2} (positive if it is away from the water surface), h_s is the convective heat transfer coefficient (Wm^{-2}K^{-1}) which relates the convective heat flux normal to the water surface to the difference between the water surface temperature (T_{ws}) and surrounding air temperature (T_a). The convective heat transfer coefficient can be estimated by (Abbasi et al., 2015):

$$h_s = 2.505 \times U_2 + 0.8520 \tag{41}$$

where h_s is in Wm^{-2}K^{-1} and U_2 in ms^{-1}, respectively. According to Abbasi et al. (2015) this equation was obtained from a CFD-based approach (CFDEvap Model) using heat and mass transfer analogy in the atmospheric boundary layer to calculate the heat and mass transfer coefficients over lake Binaba (Section 7).

Latent heat flux: latent heat flux associated with evaporation over the water surface. In general, latent heat flux is one of the most important parameters in heat dissipation, but its prediction is the most inaccurate. For the latent heat flux (H_E), the following formula is used (Abbasi et al., 2015):

$$H_E = h_m \times \rho_a(X_{ws} - X_a) \times (24 \times 3600 \times 28.4) \tag{42}$$

where the latent heat flux, H_E, is expressed in [W m^{-2}], X_a and X_{ws} are the water vapour mixing ratio of air and water surface (*kg*(*water*)/*kg* (*dry air*)), ρ_a is the air density (kg m^{-3}) and h_m is the mass transfer coefficient that is given by:

$$h_m = 0.0018544 \times U_2 + 0.0006307 \tag{43}$$

where h_m is in ms^{-1} and U_2 is in ms^{-1} respectively. X_a and X_{ws} are calculated by:

$$X_a = \frac{0.622\, e_a}{P_{atm} - e_a} \tag{44}$$

$$X_{ws} = \frac{0.622\, e_s}{P_{atm} - e_s} \tag{45}$$

where P_{atm} is atmospheric pressure (kPa), e_s is the saturation vapor pressure at the temperature of the water surface (hPa) and e_a is the vapor pressure at the air temperature (hPa) given by (Goff, 1957)

$$e_a = \left(6.11 \times \exp\left(\frac{17.27 T_a}{237.3 + T_a}\right)\right) \times \frac{RH}{100} \tag{46}$$

$$e_s = 6.11 \times \exp\left(\frac{17.27 T_{ws}}{237.3 + T_{ws}}\right) \tag{47}$$

where RH is relative humidity (%) and water surface (T_{ws}) and air (T_a) temperatures are in °C.

These heat fluxes are defined to be positive if heat flows from the water surface into the atmosphere. Heat fluxes induced by inlets and outlets and precipitation are generally disregarded (Livingstone and Imboden, 1989).

Determining correct heat fluxes for the water surface boundary is often difficult. The main difficulty is that H_{net} is a function of various parameters, where each of them has to be computed by using its own formula, which depends on many uncertain parameters (Ahsan and Blumberg, 1999; Goudsmit et al., 2002). In addition, the heat fluxes include water surface temperature (T_{ws}) that has to be calculated for each time step in advance by the model. Using this boundary condition eliminates the need for observed water surface temperature for the model.

In the current framework developed, the heat fluxes at the water surface that depend on water surface temperature, given by Eq. (39) through Eq. (47), are obtained using *groovyBC* library developed for handling the complex boundary conditions (Gschaider, 2015).

4.4.5. Inflow and outflow boundary conditions

The proposed framework is able to include the inflow and outflow boundaries in both flow and temperature simulations. In this case, the total river flow recharge or velocity and its temperature could be specified at the inflow and outflow sections. The velocities at the inflow and outflow sections are assumed to be uniformly distributed, and turbulent variables are assumed to be zero at the upstream and downstream end of the study domain. According to the measurements for the case study, during the onset of the dry season, there is no inflow and almost no outflow during the simulation period.

4.4.6. Lake-bed and lake-sides boundary conditions

In shallow lakes the temperature boundary condition at the bottom and sides could be very complex and would need extra measurements before it can be used in the model. To simulate the effects of the bottom and sides of the lake, the absorbed and reflected parts of the penetrated short-wave radiation should be measured. In addition, the heat flux from these boundaries should be specified. Using the temperature gradient or heat flux from the bed and sides can improve the simulated flow field especially in shallow lakes. In spite of the importance of these parameters, measuring these values is not easy and needs extra instrumentation that is often not available. The temperature boundary condition at the bottom of the lake and side walls depending on the available measurements for the lake, are set to zero heat flux conditions

(adiabatic condition) and can be given by (Shufen et al., 2007):

$$\frac{\partial T}{\partial z} = 0 \tag{48}$$

For the velocity boundary condition, a no flow condition is applied at the bottom and sides of the lake. Standard wall functions are used for turbulent equations in the model (Goudsmit et al., 2002; Politano et al., 2008).

5. Numerical simulation

The governing equations (Section 4.1) using the boundary and initial conditions described in Sections 4.3 and 4.4 are solved by the control-volume open-source code *OpenFOAM*. The *OpenFOAM* (Open Source Field Operation and Manipulation) toolbox includes open source $C++$ libraries released under the general public license (GPL) (OpenFOAM, 2016). Using the pre-configured built-in libraries, one can build numerical solvers for solving specific fluid flow problems (Chen et al., 2014). In the present framework, these pre-configured solvers were modified for the unsteady source/sink terms in the model equations and the buoyancy effect as described in Section 4.1.

In the current framework, a new CFD solver has been developed based on *OpenFOAM*. This is a solver for heat transfer simulation considering transient temperature source terms called *LakebuoyantBoussinesqPimpleFoam*. Besides developing the new solver, a turbulence model has been developed to include the effects of buoyancy in the flow field and wind-induced source/sink terms in turbulence.

The proposed model is an unsteady state, incompressible heat transfer solver based on the finite-volume scheme. To solve the flow, the entire desired domain has to be discretized in the vertical and horizontal directions and a proper numerical solver chosen from the pre-configured built-in algorithms in *OpenFOAM* for each of the governing equations. More details on the implemented solvers as well as numerical schemes used in this study are presented in Appendix B.

With respect to the numerical stability criteria and the transient conditions of flow in the lake, an adaptive time-stepping technique was used in the simulations which is based on Courant-Friedrick-Levy-number (CFL) (Bechmann, 2006):

$$CFL = \Delta t_{max}\left(\frac{|u|}{\Delta x}, \frac{|v|}{\Delta y}, \frac{|w|}{\Delta z}\right) \leq 1 \tag{49}$$

where u, v and w are the velocity components (ms^{-1}) in $x-$, $y-$ and $z-$directions respectively. In this study after investigating the results of the model for different sets of *CFL*, the maximum value of global *CFL* was set to 0.2. For larger values of the Courant number, the numerical computations were unstable in some points and in some time steps as well (Ferziger and Perić, 2002; Wang, 2013).

The challenges that could arise in solving these equations by running the model are memory related and simulation time. As the core of the model is based on *OpenFOAM*, the framework offers parallelization features. The model can be decomposed and run on a relatively large number of processors, either on supercomputers or HPC-Clouds.

Usually due to the limitation of computational resources, it is not possible to use a very fine mesh or very small time steps in simulations. In this study different settings for numerical schemes and mesh sizes as well as the time steps were considered to find the optimal balance between the needed computational resources and the desired accuracy. For example in the case of lake Binaba, the time step values varied between 0.1 and 10.0 s(i.e. $0.1 \leq \Delta t \leq 10.0$ s) and four days of simulations, as described in Section 7.2, took about 20 h on the HPC Cloud-based virtual machine with 12 Intel processors at 2.7 GHz and 96GB RAM (Collaborative Organisation for ICT in Dutch Higher Education and Research, 2016).

6. Post-processing phase

At the post-processing stage, the boundary conditions, mathematical issues, computational grid, etc. are to be verified. In addition, the desired parameters and functions which are needed for analysing the flow field and temperature distribution have to be obtained.

6.1. Model validation

One of the principle objectives in the current framework is to obtain general information on the direction and magnitude of the currents in the water bodies and the temperature dynamics, and how they vary over time. Once the simulations are validated, it is possible to use the model for different conditions that could be used to describe in general terms the most significant patterns in the water currents' variations over time. One of the big challenges in validating lake models such as the one in this study is the fact that experimental data are rarely available and/or measurement errors are high (Callister, 2008).

Several assumptions are made in the development of the lake model regarding the input values. The results from the simulations are plotted against the measured data as a way to evaluate the validity of the model (Callister, 2008). To validate the model, different cases were run to check the performance of different components of the framework. Using different case studies with different conditions allows the user to easily identify problems with the model and be able to modify the model in a straightforward manner.

6.1.1. Convection heat transfer in the water body

Due to the long running time of the real geometry, it is reasonable to validate the model with some simple geometries to be sure about its performance. It should be noted that in the case studies discussed, the physics of the simulations and the general trends of the results are investigated which are very helpful in debugging the model.

The first case described here deals with a 2-D flow in a cavity shown in Fig. 5. Using this case, the performance of the model in simulating heat transfer in the cavity (natural convection) was validated. To evaluate the performance of the model developed in this study, the results of the cavity model using the current approach were compared with some available flow parameters for the cavity model in similar conditions such as the results of the simulation by Corzo et al. (2011) and the benchmark experimental measurements done by Le Quéré (1991). Fig. 6(a) shows the horizontal velocity profile ($u = U_x/\alpha$) in the vertical mid-line. These results exhibit good agreement between the model with benchmark results. However, the quality of results are dependent on the computational grid and it is necessary to refine the grid in order to obtain an accurate solution. In Fig. 6(b) the vertical profiles of the velocity are shown. Comparison of the temperature distribution shown in Fig. 6(c) with velocity profile shown in Fig. 6(d) shows that the flow is limited to a narrow strip along the walls (left hot wall and right cold wall) where the velocity and temperature change suddenly.

6.1.2. Simplified geometry of water body

In this section the ability of the framework in taking into consideration the effects of forced convection (heat transfer) in the water body is verified. As mentioned in Section 4.1 the temperature source term in the water is a function of the water turbidity. To check the performance of the model for different turbidity values and also to investigate the magnitude of the turbidity effects on the flow and temperature pattern in small and shallow water bodies, some simulations were done and the results have been analysed. In addition the influence of turbulence on the results was examined. The details of these test cases are listed in Table 3. As shown, two different geometries (*S* and *L* cases) are considered to check the performance of the model in solving the flow field in the simple geometries with different dimensions of water bodies.

In Fig. 7(a) the simulated temperature profiles in the water body (*S*

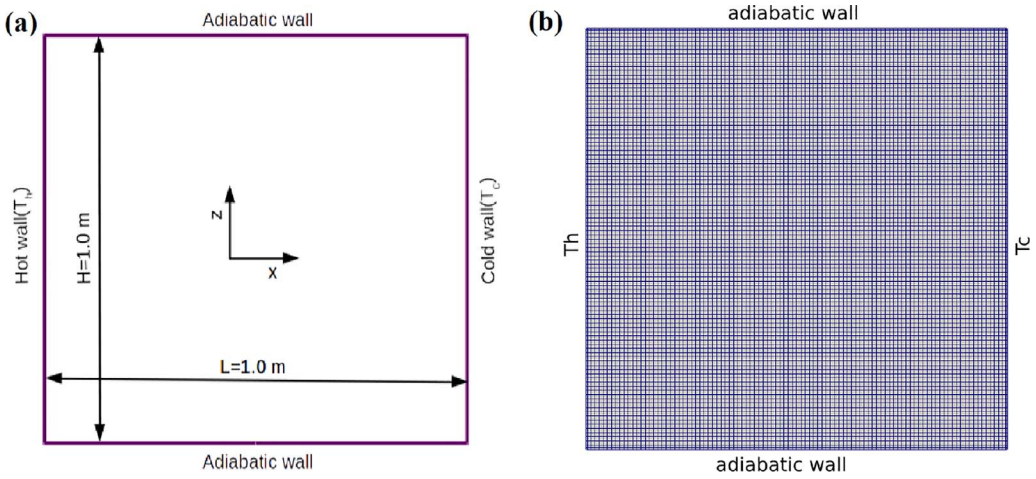

Fig. 5. Detail of the validation case (cavity) where T_c = 303.15 K and T_h = 304.15 K: **(a)** geometry and model's conditions; **(b)** computational grid.

cases) for different water turbidity values are shown. It shows that the effect of Secchi depth in the shallow water bodies could be significant and should be considered in models. Fig. 7(b) shows the temporal variations of temperature in the water body for case *S-03*. The temperature distribution in the water correlates highly with the air temperature and at sometimes there is distinct stratification in the lake. In Fig. 7(c), the simulated temporal variations of temperature in the water body without considering the turbulence in the simulations case *S-01*is compared with Fig. 7(d) which includes the turbulence in modeling case *S-05*. It shows that the effects of the turbulence in the flow field could be significant. Ignoring the turbulence in the simulation leads to unreliable results which give no stratification in the water body.

In the second simplified geometry case (*L* case), the larger dimensions similar to the real lake dimensions were chosen for the computational domain to investigate the performance of the framework in working with real dimensions. The real dimensions allow one to improve and handle the mathematical and computational issues such as selecting the proper numerical algorithm and required computational resources. Fig. 8(a) shows the temperature profile in the case study for different values of water turbidity. According to the results, in order to have better predictions on stratification in shallow lakes, it is important to measure the Secchi depth in some points in the water body. Using the measured water turbidity values in the model could increase the reliability of the results. In Fig. 8(b) the distribution of the velocity's components in the water body are shown case *L-02*. It shows that in the water body, the velocity distribution is a function of the wind speed over the water surface and its direction as well. In addition, according to the velocity distributions in Fig. 8(b), there are water flows in the

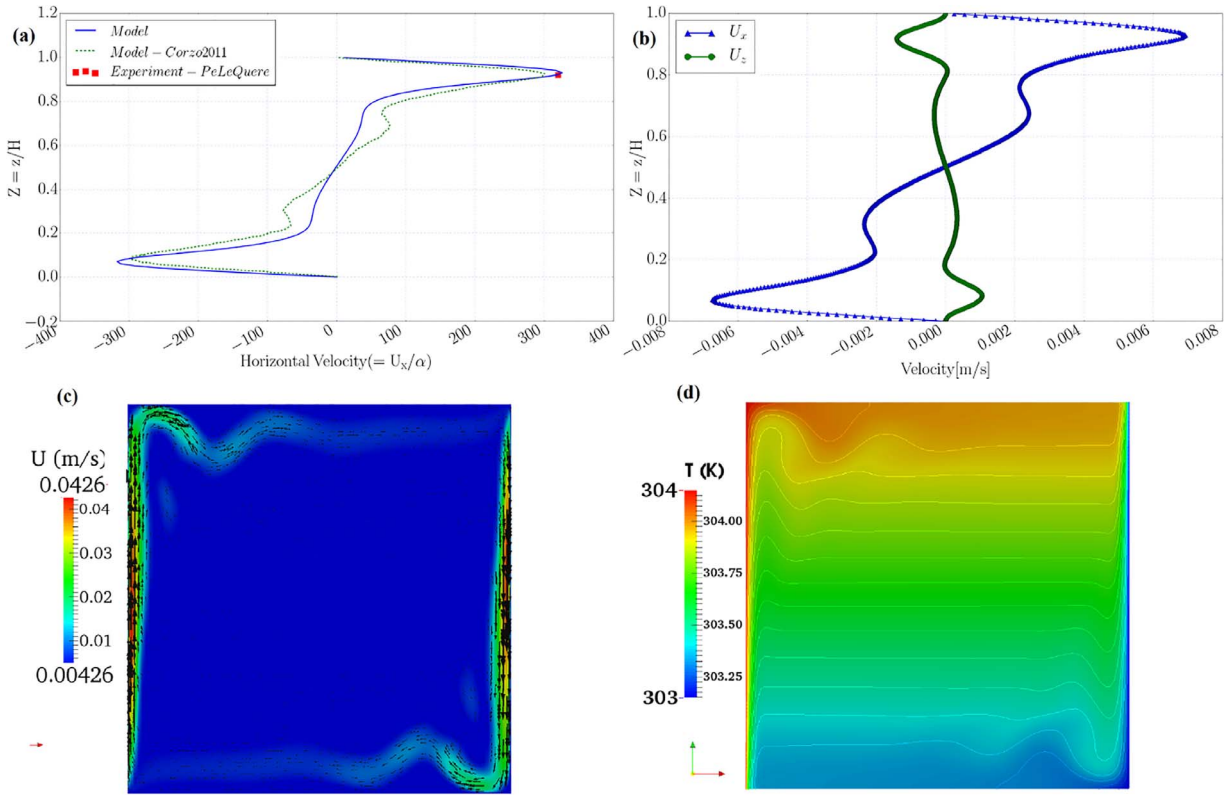

Fig. 6. Results of the model in the cavity: **(a)** comparison of the results of the model (horizontal velocity profiles, $u = U_x/\alpha$, at x mid-plane where $Ra = 10^8$; Ra is Rayleigh number) with experimental values and other models; **(b)** simulated profiles of the velocity components in the cavity; **(c)** simulated velocity vectors and the values at x mid-plane; and **(d)** temperature distribution and the contours in the cavity.

Table 3
Details of simplified case studies.

Case ID	Dimensions $L \times W \times H$ [m]	Cells Number	Δx [m]	Δy [m]	Δz [m]	z_{min} [m]	aspect ratio	η m^{-1}	Secchi depth[m]	Remarks
S-01	120 × 100 × 4	6'000	10.0	10.0	0.2	0.2000	50.08	0.50	2.94	Laminar flow(no turbulence)
S-02	120 × 100 × 4	12'000	5.0	5.0	0.2	0.0125	800.00	1.82	0.50	Turbulent Flow
S-03	120 × 100 × 4	12'000	5.0	5.0	0.2	0.0125	800.00	3.56	0.20	Turbulent Flow
S-04	120 × 100 × 4	12'000	5.0	5.0	0.2	0.0125	800.00	5.17	0.12	Turbulent Flow
S-05	120 × 100 × 4	12'000	5.0	5.0	0.2	0.0125	800.00	4.20	0.16	Turbulent Flow
L-01	1000 × 800 × 4	46'000	20.0	20.0	0.2	0.0250	800.00	2.10	0.41	Turbulent Flow
L-02	1000 × 800 × 4	46'000	20.0	20.0	0.2	0.0250	800.00	4.20	0.16	Turbulent Flow
L-03	1000 × 800 × 4	46'000	20.0	20.0	0.2	0.0250	800.00	10.00	0.05	Turbulent Flow
L-04	1000 × 800 × 4	46'000	20.0	20.0	0.2	0.0250	800.00	2.10	0.41	Turbulent Flow, $S_T = 0$

water body in different directions and this could increase the circulation in the water body. In Fig. 8(c,d) the effects of water turbidity on the temporal distribution of temperature for cases *L-01* and *L-03* cases are shown, respectively. It can be seen that turbidity could affect the temperature distribution in the water body and its actual values or best estimates should be used.

To check the performance of the model including the source/sink terms some simulations were done. In Fig. 9(a) and (b) the velocity and temperature changes at different depths are shown. As shown, the results are not so good compared with the validated model. The main reasons could be related to the low wind velocity values and the complex geometry of the lake (Wang et al., 2013). Therefore, in the case of shallow lakes with low wind velocity values, this approach is not suggested.

Following the approach described in Section 4.4.1 the heat flux boundary condition was applied to the water surface and the changes of velocity and temperature are shown in Fig. 9(c) and (d) respectively. The differences between the temperature values in this simulation with the validated case could be due to the uncertainties that exist in estimating the heat fluxes values at the water surface as well as the dependency of the temperature gradient on the water-air interface on the flow parameters such as heat conductivity (Eqs. (6) and (36)). In this approach, the assigned right boundary conditions for turbulent equations are important and their values would affect the results of the model significantly.

7. Model application for lake Binaba

To check the performance of the framework developed in this study, it has been applied for a real small shallow lake. All described steps in the framework were followed to generate the bathymetry, set-up the boundary conditions and run the model.

7.1. Site description and measurement methodology

Lake Binaba is a small shallow man-made reservoir located in the Upper East Region of Ghana. The Upper East Region of Ghana (UER) has more than 160 small shallow reservoirs which have different

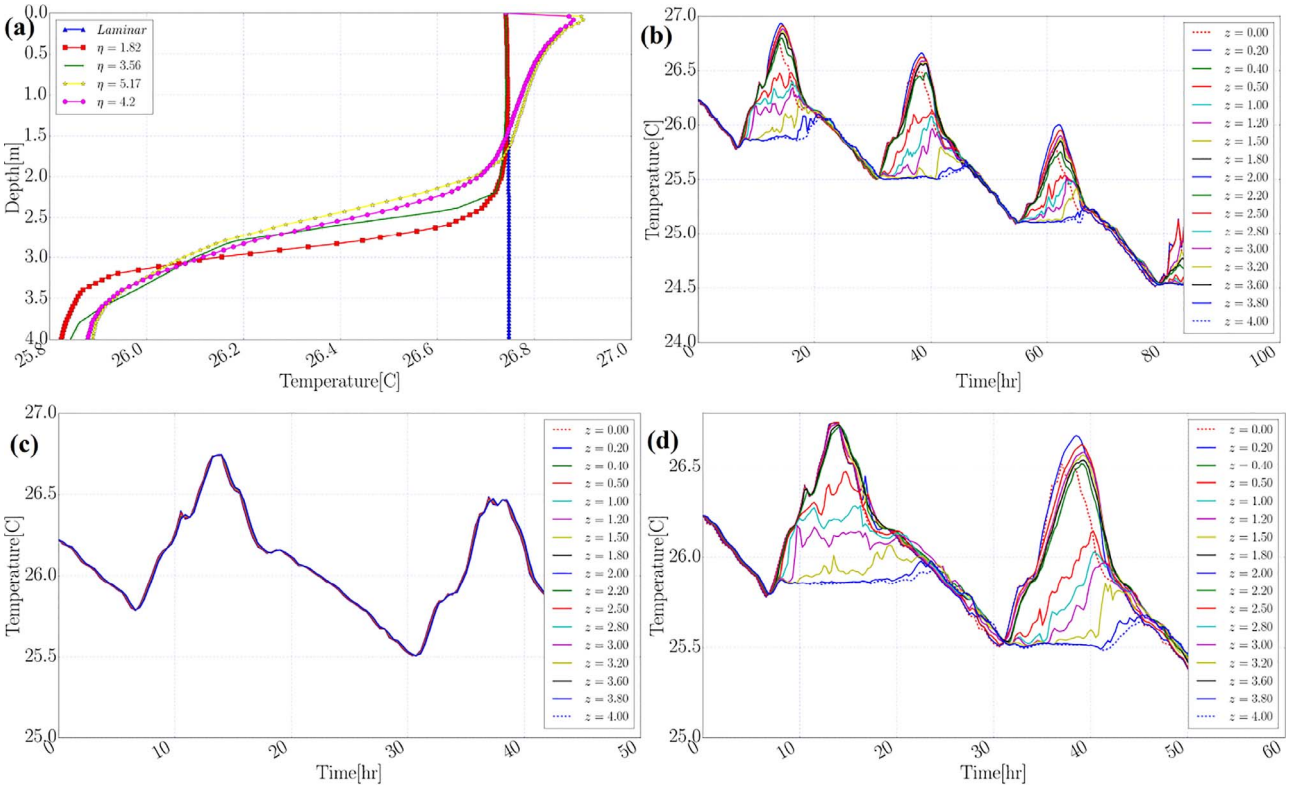

Fig. 7. Results of the model for S cases: **(a)** effect of turbidity on vertical temperature profiles in the water body; **(b)** temporal variation of temperature for the selected turbidity value (case S-03 where $\eta = 3.56$ m^{-1}); **(c)** simulated temporal temperature variations in the water body without turbulence implementation (laminar assumption) for case S-01; **(d)** temporal temperature consider the turbulence in the simulation (case S-05 where $\eta = 4.2$ m^{-1}).

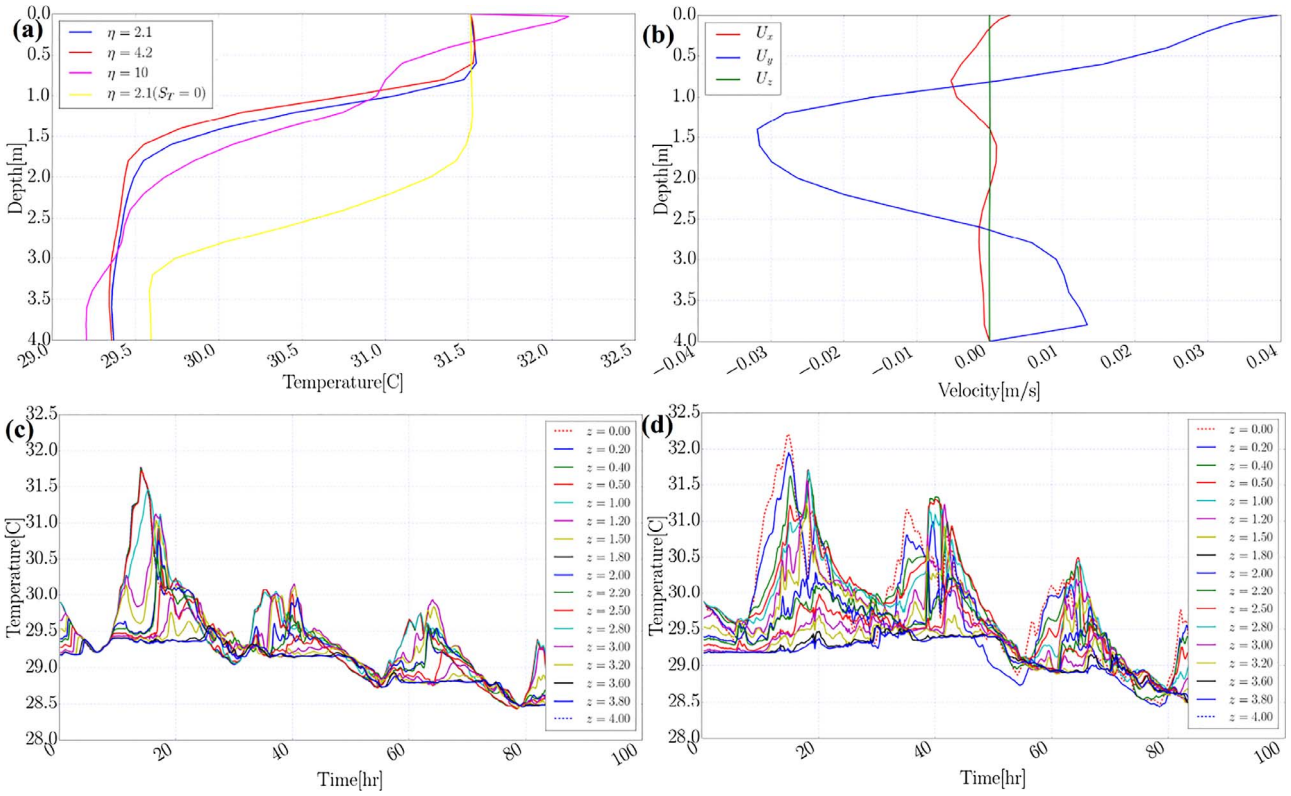

Fig. 8. Results of the model for L cases: **(a)** effect of turbidity on vertical temperature profiles in the water body; **(b)** velocity's components distribution in the water body for case *L-02* where $\eta = 4.2$ m^{-1}; **(c),(d)** simulated temporal variation of temperature in the water body for different water turbidity values where $\eta = 2.1$ (case L-01) and $\eta = 10.0$ m^{-1} (case L-03) in (c) and (d) respectively.

surface areas ranging from 1.0 to 100.0 ha (Annor et al., 2009). These small reservoirs have the advantage of being operationally efficient with their flexibility, closeness to the point of use, and requirement for few parties for their management. Lake Binaba (10°53′20″N,00°26′20″W) is used for fishing, livestock watering, irrigation, construction, domestic uses and recreation (van Emmerik et al., 2013). The average area of the lake surface is 31 ha (305,534 m^2) with the average and maximum depth of 1.1 m and 4.0 m, respectively (Abbasi et al., 2017). The length of lake in $x-$direction (length) is around 900.0 m and in $y-$direction (width) is 600.0 m. The temperature profile in the water body as well as the micrometeorological parameters were measured at a floating measurement station over the water surface. (Fig. 10)

The atmospheric parameters needed as input in the model should be measured. The standard climatic parameters, including air temperature, relative humidity, wind speed and wind direction, were recorded at a height of 2.0 m above the water surface. The floating measurement platform had a solar radiation sensor (model PYR from Decagon Devices, USA; ± 5%) for solar radiation flux density (Wm^{-2}) measurement, a humidity/temperature sensor (model VP-4 from Decagon Devices, USA; ± 2% and ± 0.25 °C for humidity and temperature, respectively) for air humidity measurement and air temperature, and a sonic anemometer (model DS2 from Decagon Devices, USA; ± 3% and ± 3.0° for wind speed and wind direction, respectively) to measure wind speed and its direction. The micro-climatic parameters (air temperature, relative humidity, wind speed and its direction) were averaged at 5-min intervals and used as input values in the lake model.

Water surface temperature and the vertical temperature profile in the water body have been measured during the study period. The temperature values were measured using HOBO tidbit v2 temperature loggers with nominal accuracy of ± 0.21 °C and at the following depths: 0.0 (water surface), 0.100, 0.200, 0.500, 1.100, 1.550, 1.850, 2.150, 2.800, and 3.465 m. The measured temperature values were used to validate the model results. The air temperature fluctuated from 18.0 to 40.0 °C with an average of 28.7 °C while the water surface temperature varied between 24.0 °C and 32.5 °C with an average of 27.5 °C during the measurement period. Measurements were done between 23 November 2012 and 22 December 2012. A four-day period was selected randomly from the observations for use in lake model. For more details, the reader is refereed to Abbasi et al. (2016a).

The bathymetric survey was carried out using a boat, Raymarine Dragonfly 7 depth/fish finder (for depth measurement) and a handheld Garmin etrex 20 GPS device (for the location of the depth measurement) bearing in mind the need to make the field campaign cost-effective for the developing countries (GARMIN, 2016; Raymarine, 2016). The measured data set, which consists of *x, y*, and *z*(depth) values, was called "initial point-cloud". This initial point-cloud has been used to generate the geometry of the lake as described in details in Section 3.1.

7.2. Model results for lake Binaba

The lake model was run for four days (345,600 s) for lake Binaba. The starting time of simulation was 12:00:00 a.m. on 24 November 2012. Fig. 11(a) shows the geometry of lake Binaba generated by using the proposed approach in the current platform (Section 3.1). In Fig. 11(b) the computational grid of the lake is shown. The computational grid is refined near the water surface due to high gradients in the temperature and velocity over the water surface. The simulated velocity values and the temperature contours in 1.0 m beneath the water surface are shown in Fig. 11(c) and (c) respectively. The distribution of temperature, as shown in Fig. 11(d), at a depth of 1.0 m below the water surface is not homogeneous mainly due to the non-homogeneous distribution of velocity at this depth (Fig. 11(c)). In Fig. 12 the simulated velocity vectors on the water surface is depicted and shows the existence of inverse flow which enhances circulation in the water body. As this framework can work with complex boundary conditions, the effects

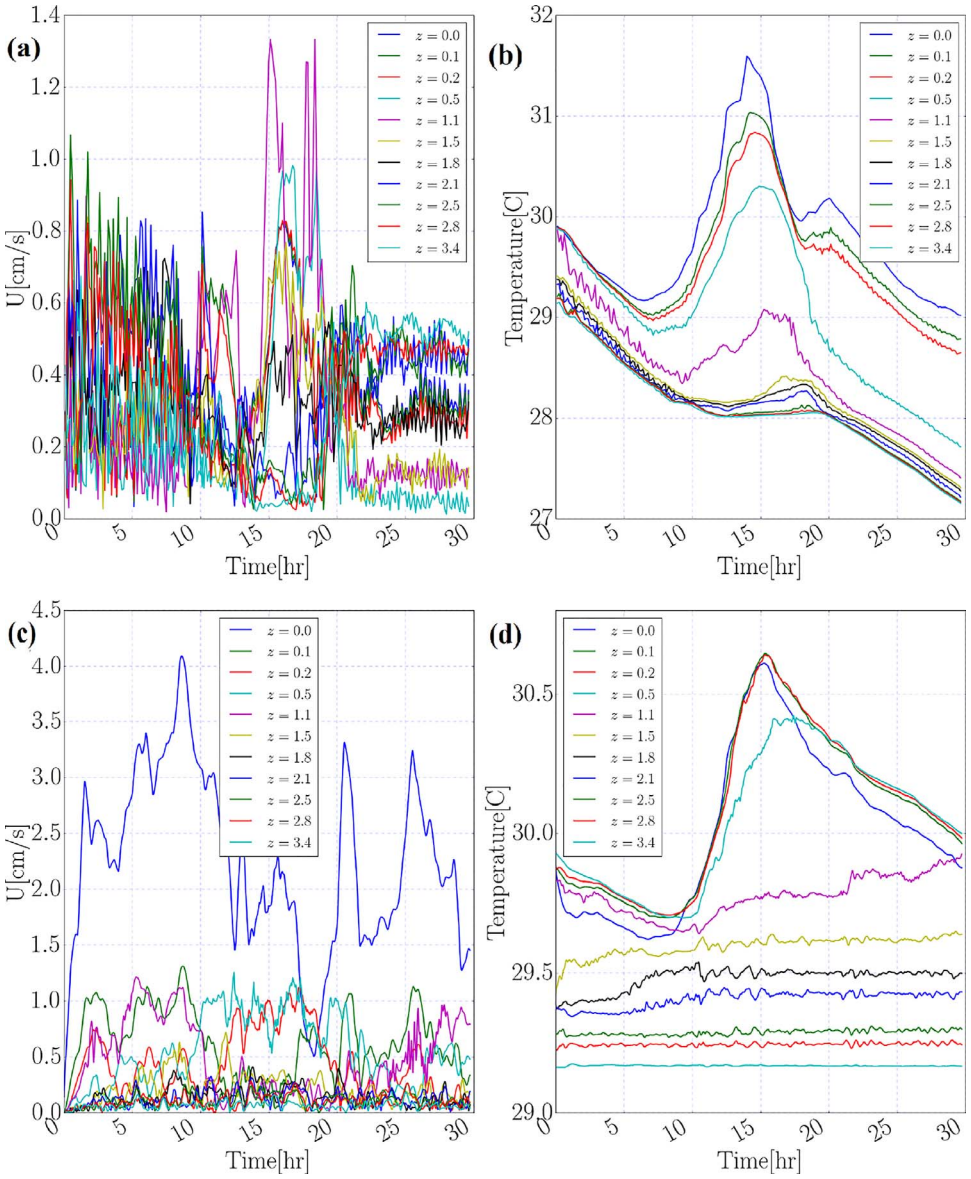

Fig. 9. Results of the model considering different approaches to include the wind velocity effects: **(a), (b)** temporal distribution of velocity and temperature values respectively, when the effects of wind are considered as source/sink terms in turbulence equations; **(c),(d)** temporal distribution of velocity and temperature values respectively, when the effects of wind speed are considered as shear stress boundary condition over the water. In both cases, the heat flux temperature boundary condition are assumed over the water surface.

Fig. 10. The shape of lake Binaba and its surroundings (Google, 2015). Location of the floating measurement platform is shown by the filled red square. (For interpretation of the references to color in this figure legend, the reader is referred to the web version of this article.)

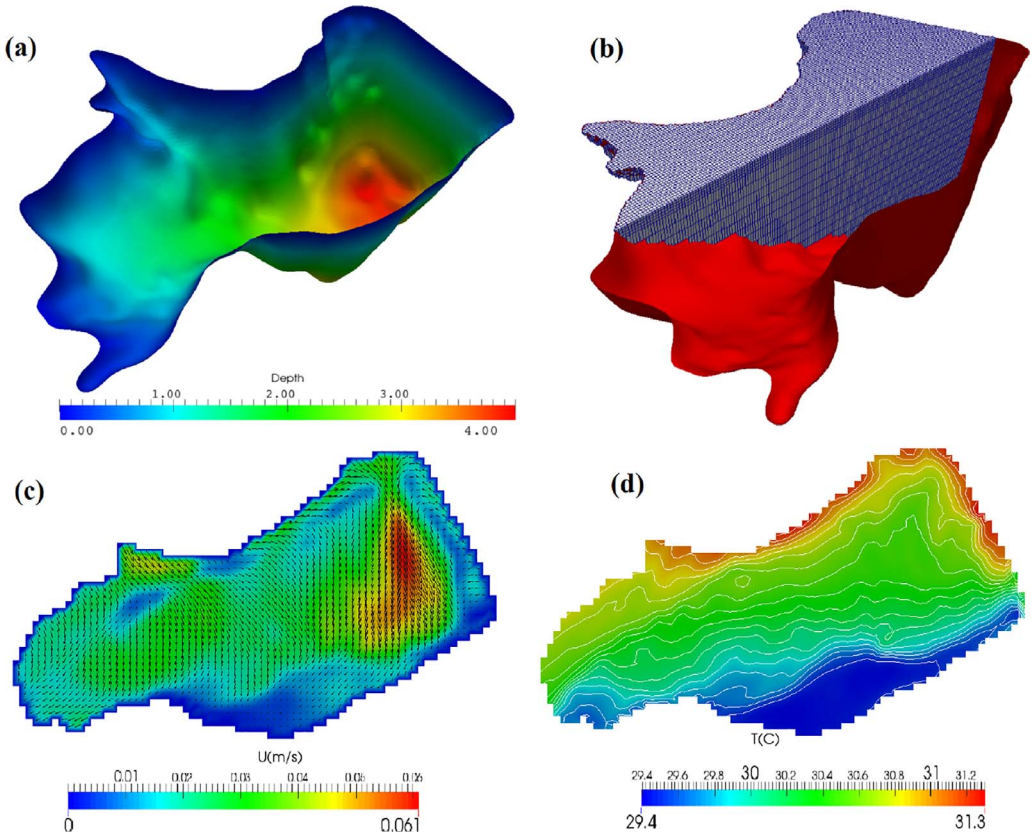

Fig. 11. **(a)** The generated geometry of Lake Binaba with depth distributions; **(b)** computational grid in the water body to use in simulation (vertical exaggerated by 100); **(c)** simulated velocity field (stream lines); and **(d)** temperature field (values and contours) in 1.0 meter beneath the water surface at $t = 13{:}00$ h. The wind speed is 2.0 ms^{-1} from South-West.

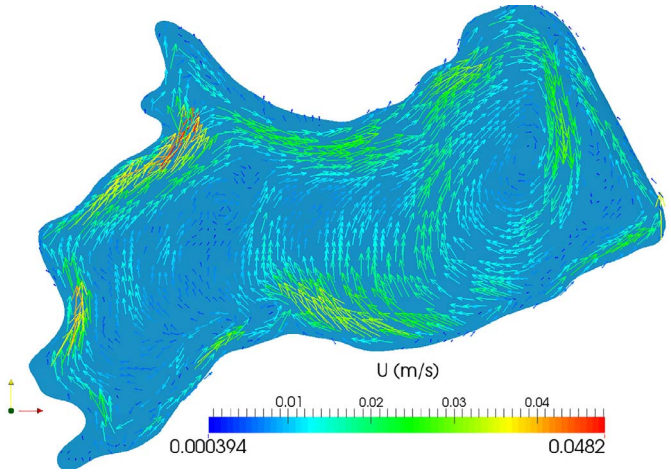

Fig. 12. Simulated velocity vectors and velocity magnitudes on the water surface at $t = 17{:}00$ h. The wind speed is 2.1 ms^{-1} from South-West.

of the lake surroundings can be accounted in the results. For example, the effect of advection, which is important in (hot) arid and semi-arid regions, has been implemented in the water surface boundary conditions implicitly as heat fluxes over the water surface. This type of advection is different from the one happens inside the water body which is included in the governing equations as described in Section 4.1 and implemented in Eq. (2) as $\frac{\partial}{\partial x_j}(u_j u_i)$. More details about the validation process and analysing the model results can be found in Abbasi et al. (2016a).

8. Conclusion

In this study, a comprehensive framework for simulating small shallow inland water bodies was developed. This framework includes all mandatory steps in small shallow water bodies modeling which includes: creating bathymetry, generating computational grid, solving the flow field and temperature dynamics, plotting desired graphs, and analyzing the outputs. In order to produce a precise geometry applicable in CFD simulations, a new generalizable and cost-effective approach using open-source tools has been developed which could be easily implemented. Moreover, to consider the buoyancy effects in the water body, the turbulence model was improved to take into account the buoyancy effects. Considering the commonly available measurements for small water bodies, a wide range of boundary conditions are proposed that can be adapted to suit the measurements at hand over the water surface. To check the performance of the framework, several test cases and a real-world lake were simulated and compared with field measurements.

Applying the framework developed in this study for different model configurations, for instance using different boundary conditions, turbulence models, source term in temperature equation, and lake characteristics, has led to the following conclusions.

1. Compared to deep lakes, the interaction between the flow and temperature dynamics is more critical for shallow lakes. Therefore, to estimate both flow variables and temperature accurately in shallow water bodies, coupling energy and momentum is mandatory. Although coupling of heat transfer processes with water flow in the lake commonly gives more accurate results, stability and accuracy of the results are sensitive to the numerical algorithms chosen in the simulations.
2. Temperature dynamics and flow pattern in the water are determined by the atmospheric conditions over the water surface (i.e. micrometeorological parameters such as air temperature, incoming shortwave radiation, wind velocity and its direction, etc.). Therefore, the accuracy of the model results depends on the errors and uncertainties in the observed micrometeorological parameters which are used as boundary conditions. Calculating accurate values of heat

flux components over the water surface, especially for latent heat flux (evaporative heat flux), which are required as temperature boundary conditions, is challenging and includes a high degree of uncertainty.
3. The model results, especially near the free water surface, are sensitive to the spatial and temporal resolutions used in the simulations. Finding a reasonable balance between the computational mesh and the required computational resources (i.e. optimizing the computational grid) is an important and time-consuming step in simulating lake-like domains.
4. Using open-source tools to develop a flexible framework for simulating small shallow water bodies is promising, because they do not require commercial licenses. Hence, they can be used in developing countries for the management of water (quantity and quality) stored in small shallow lakes.

A wide range of model configurations has been described in this study. Picking out the right turbulence model and boundary conditions is very important and can affect the results significantly. It is obvious that using methods with less uncertainties, if possible, are better in computing the parameters because they give better results. Finally, the framework developed in this study for temperature dynamics can be applied to water quality, biological and environmental simulations of shallow water bodies.

Acknowledgments

This work was carried out on the Dutch national e-infrastructure with the support of SURF Foundation (under grant number e-infra140092). The work was also supported by Challenge Program on Water and Food (CPWF), the European Space Agency's TIGER project and the SOAR-Africa project by the Canadian Space Agency (CSA).

Appendix A. RKE turbulence model equation

A wide range of turbulence models have been developed in CFD simulations. From literature reviewed, standard $k-\varepsilon$ (SKE) and realizable $k-\varepsilon$ (RKE) models are widely used in most CFD simulations. The semi-empirical standard $k-\varepsilon$ model contains transport equations for the turbulence kinetic energy (k) and the dissipation rate of kinetic energy (ε). Various two-equation models, such as $k-\omega$, similar to the standard $k-\varepsilon$ model are available which need extra input parameters. However the standard $k-\varepsilon$ model is mostly used for circulation models with free surface variation. According to the literature review and investigating similar simulations for coupling heat transfer and flow dynamics, it was found that the implemented realizable $k-\varepsilon$ model provides better results than other $k-\varepsilon$ models (Section 4.2). In fact, the word 'realizable' implies that the model is based on particular mathematical constraints on the Reynolds stresses and compatible with the physics of turbulent flows.

In realizable $k-\varepsilon$ models, the turbulent kinetic energy (k in m^2s^{-2}) and the dissipation rate of turbulent kinematic energy (ε in m^2s^{-3}) are obtained from Eqs. (12) and (13) respectively. In these equations, the parameter $C_{\varepsilon 3}$ (dimensionless) is the ratio of the velocity functions in the vertical and longitudinal directions and is not constant but instead depends on the flow conditions (Lee, 2007):

$$C_{\varepsilon 3} = \tanh\left|\frac{w}{u_h}\right| \tag{A.1}$$

where u_h and w are the components of the flow velocity perpendicular and the components of the flow velocity parallel to the gravitational vector, respectively (ms^{-1}). The coefficient C_1 is evaluated as (Shih et al., 1995):

$$C_1 = max\left(0.43, \frac{\zeta}{\zeta+5}\right) \tag{A.2}$$

$$\zeta = S\frac{k}{\varepsilon} \tag{A.3}$$

$$S = \sqrt{2S_{ij}Sji} \tag{A.4}$$

$$S_{ij} = \frac{1}{2}\left(\frac{\partial u_i}{\partial x_j} + \frac{\partial u_j}{\partial x_i}\right) \tag{A.5}$$

and the turbulent kinematic viscosity is given by

$$\nu_T = C_\mu \frac{k^2}{\varepsilon} \tag{A.6}$$

$$C_\mu = \frac{1}{A_0 + A_s\frac{kU^*}{\varepsilon}} \tag{A.7}$$

$$U^* = \sqrt{S_{ij}S_{ji} + \overline{\Omega_{ij}}\,\overline{\Omega_{ij}}} \tag{A.8}$$

$$A_s = \sqrt{6}\cos\phi \tag{A.9}$$

$$\phi = \frac{1}{3}cos^{-1}(\sqrt{6}W) \tag{A.10}$$

$$W = \frac{S_{ij}S_{jk}S_{ki}}{\widetilde{S}^3} \tag{A.11}$$

$$\widetilde{S} = \sqrt{S_{ij}S_{ij}} \tag{A.12}$$

where $\overline{\Omega_{ij}}$ is the mean rate-of-rotation tensor. The production of turbulent kinetic energy by the mean velocity gradient (G_k) is written as

$$G_k = \nu_t S^2 \tag{A.13}$$

Appendix B. Implemented numerical schemes

In Table B.1 the list of applied solvers is presented. These solvers are selected based on their stability, convergence and processing time after trying a number of simulations. Throughout this work, the *Euler* method was used to discretize the temporal term. This is a first-order, bounded implicit method and the *SmoothSolver* for the momentum, k, ε and T equations is used with a *GaussSeidel* smoother (Gauss refers to the standard finite volume discretization of Gaussian integration). The *GAMG* (Geometric-algebraic multi-grid) solver is chosen for the pressure equation. This solver generates an initial quick solution using a coarse mesh with a small number of cells, and maps this solution onto a finer mesh. The quick solution is used as an initial guess to obtain an accurate solution on the fine mesh. Therefore, *GAMG* is generally faster than other standard methods. For the spatial discretization of differential operators, the *Gaussian* integration was used with various interpolation schemes: for gradient terms, the 2nd

Table B.1
Solution algorithms used in the framework developed for CFD calculations (Maric et al., 2014).

	Field	Task	Solver	Description
1	Pressure, corr. pressure pd	solver	PCG	Preconditioned conjugate gradient solver
		preconditioner	GAMG	Generalised geometric-algebraic multi-grid
2	Velocity	solver	PBiCG	Preconditioned bi-conjugate gradient solver
		preconditioner	DILU	Diagonal incomplete-LU
3	cell motion cellMotionU	solver	PCG	Preconditioned conjugate gradient solver
		preconditioner	DIC	Diagonal incomplete-Cholesky

Table B.2
Numerical schemes chosen for CFD calculations of the SSL-framework (Maric et al., 2014).

	Item	Symbol	Keyword	Description
1	First and second time derivatives	$\frac{\partial}{\partial t}$	Euler	First order, bounded, implicit
2	Gradient	∇	faceLimited leastSquares 0.5	Limited, second order least squares
3	Divergence (velocity terms)	$\nabla . \vec{u}$	Gauss vanLeerV	Second order Gaussian integration, van Leer interpolation for face centres
4	Divergence (phase fraction terms)	$\nabla.\gamma$	Gauss vanLeerV	As 3, strictly bounded between 0 and 1
5	Laplacian	∇^2	Gauss linear corrected	Second order, Gaussian integration, linear interpolation for face centres, conservative
6	Point-to-point interpolation		linear	Linear interpolation for general field
7	Gradient component normal to face	∇_{SN}	corrected	Explicit non-orthogonal correction

order linear interpolation, for divergence terms, the 2nd order upwind interpolation and for Laplacian terms, the 2nd order linear interpolation with explicit non-orthogonal corrections. Table B.2 shows the main numerical methods which could give stable and converged solutions in small shallow water body simulations. To improve the stability of the computations, the relaxation parameters, which controls under-relaxation, were set to 0.3 for pressure and 0.5 for the other variables. Under-relaxation parameters control the variable changes from one iteration to the next.

The *PIMPLE* method was used for pressure-velocity coupling. The *PIMPLE* algorithm combines the *SIMPLE* (Semi-Implicit Method for Pressure-Linked Equations) algorithm and the *PISO* (Pressure Implicit with Splitting of Operators) algorithm to rectify the second pressure correction and correct both velocity and pressure explicitly. This algorithm allows one to use larger time steps than the *PISO* algorithm.

References

Abbasi, A., Annor, F.O., van de Giesen, N., 2015. Developing a CFD-based approach to estimate evaporation from water surfaces in (semi-)arid regions. Hydrol. Process. (Manuscript re-submitted for publication).

Abbasi, A., Annor, F.O., van de Giesen, N., 2016. Investigation of temperature dynamics in small and shallow reservoirs. case stuy: lake binaba, upper east region of ghana. Water 8 (3), 1–24.

Abbasi, A., Annor, F.O., van de Giesen, N., 2016. The effects of small water surfaces on turbulent flow in the atmospheric boundary layer: URANS approch implemented in openfoam. Environ. Modell. Softw. (Manuscript submitted for publication).

Abbasi, A., Annor, F.O., van de Giesen, N., 2017. Effects of atmosphere stability conditions on heat fluxes from small water surfaces in (semi-) arid regions. Hydrol. Sci. J. 62 (9), 1422–1439. http://dx.doi.org/10.1080/02626667.2017.1329587.

Abeysinghe, K., Nandalal, L., Piyasiri, S., 2005. Prediction of thermal stratification of the kotmale reservoir using a hydrodynamic model. J. Nat. Sci. Found. 33 (1), 25–36.

ADMesh, 2016. ADMesh[online]. Available from: http://www.varlog.com/admesh-htm. [Accessed 14 November 2016].

Ahsan, A.K.M.Q., Blumberg, A.F., 1999. Three-dimensional hydrothermal model of onondaga lake, new york. J. Hydraul. Eng. 125 (9), 912–923.

Annor, F.O., van de Giesen, N., Liebe, J., van der Zaag, P., Tilmant, A., Odai, S., 2009. Delineation of small reservoirs using radar imagery in a semi-arid environment: A Case study in the upper east region of ghana. Phys. Chem. Earth. 34 (4–5), 309–315. http://dx.doi.org/10.1016/j.pce.2008.08.005.

ANSYS, 2016. ANSYS Fluent[online]. Available from: http://resource.ansys.com/Products/Simulation+Technology/Fluid+Dynamics/Fluid+Dynamics+Products/ANSYS+Fluent. [Accessed 14 November 2016].

Appt, J., Imberger, J., Kobus, H., 2004. Basin-scale motion in stratified upper lake constance. Limnol. Oceanogr. 49 (4), 919–933.

Bartzanas, T., Kacira, M., Zhu, H., Karmakar, S., Tamimi, E., Katsoulas, N., Lee, I.B., Kittas, C., 2013. Computational fluid dynamics applications to improve crop production systems. Comput. Electron. Agric. 93, 151–167.

Bechmann, A., 2006. Large-Eddy Simulation of Atmospheric Flow over Complex Terrain.

Risø National Laboratory, Technical University of Denmark Thesis(PhD).
Bednarz, T.P., Lei, C., Patterson, J.C., 2008. Unsteady natural convection induced by constant surface cooling in a reservoir. Austr. New Zealand Industr. Appl. Mathe. J. 48, 852–867.
Bednarz, T.P., Lei, C., Patterson, J.C., 2009. Unsteady natural convection induced by diurnal temperature changes in a reservoir with slowly varying bottom topography. Int. J. Therm. Sci. 48, 1932–1942. http://dx.doi.org/10.1016/j.ijthermalsci.2009.02.011.
Bigham Stephens, D.L., Carlson, R.E., Horsburgh, C.a., Hoyer, M.V., Bachmann, R.W., Canfield, D.E., 2015. Regional distribution of secchi disk transparency in waters of the united states. Lake Reserv. Manag .31, 55–63. http://dx.doi.org/10.1080/10402381.2014.1001539.
Branco, B.F., Torgersen, T., 2009. Predicting the onset of thermal stratification in shallow inland water bodies. Aquat. Sci. 71 (1), 65–79. http://dx.doi.org/10.1007/s00027-009-8063-3.
Brockhaus, G.T., 2011. Hydrodynamic Design of Ship Bulbous Bows Considering Seaway and Operational Conditions. Technischen Universit at Berlin Thesis(PhD).
Callister, E.V., 2008. A Three-Dimensional, Time-Dependent Circulation Model of Utah Lake. Utah State University Thesis(MSc).
Casulli, V., 1997. Numerical simulation of three-dimensional free surface flow in isopycnal co-ordinates. Int. J. Numer. Methods Fluids 25, 645–658.
Casulli, V., 1999. A semi-implicit finite difference method for non-hydrostatic, free-surface flows. Int. J. Numer. Methods Fluids 30, 425–440.
Casulli, V., Cheng, R.T., 1992. Semi-implicit finite difference methods for three-dimensional shallow water flow. Int. J. Numer. Methods Fluids 15, 629–648.
Charnock, H., 1955. Wind stress on a water surface. Q. J. R. Meteorol. Soc. 81 (350), 639–640.
Chen, G., Xiong, Q., Morris, P.J., Paterson, E.G., Sergeev, A., Wang, Y.-C., 2014. OpenFOAM for computational fluid dynamics. Not. Am. Math. Soc. 61 (4), 354. http://dx.doi.org/10.1090/noti1095.
Chen, X., 2003. A free-surface correction method for simulating shallow water flows. J. Comput. Phys. 189, 557–578. http://dx.doi.org/10.1016/S0021-9991(03)00234-1.
Chen, X., 2003. A fully hydrodynamic model for three-dimensional, free-surface flows. Int. J. Numer. Methods Fluids 42, 929–952.
Chen, Y., Wai, O.W.H., Li, Y.S., 2003. Numerical model for wave refraction-diffraction near pearl river estuary, china. J. Waterway, Port, Coastal, Ocean Eng. 129 (6), 260–269.
Chen, Z., Han, S., Zhou, F.-Y., Wang, K., 2013. A CFD modeling approach for municipal sewer system design optimization to minimize emissions into receiving water body. Water Resour. Manage. 27 (7), 2053–2069.
Collaborative Organisation for ICT in Dutch Higher Education and Research, 2016. SURFsara[online]. Available from: https://www.surf.nl/en/services-and-products/hpc-cloud/technical-specifications/index.html. [Accessed 15 November 2016].
Corzo, S.F., Damián, S.M., Ramajo, D., Norberto, M.N., 2011. Numerical simulation of natural convection phenomena. Mecánica Computacional XXX, 277–296.
Craig, P.D., Banner, M.L., 1994. Modeling wave-enhanced turbulence in the ocean surface layer. J. Phys. Oceanogr. 24, 2546–2559.
Deltares, 2016. Delft3D[online]. Available from https://oss.deltares.nl/web/delft3d. [Accessed 14 November 2016].
Elo, A.-r., 2007. The energy balance and vertical thermal structure of two small boreal lakes in summer. Boreal Environ. Res. 12, 585–600.
van Emmerik, T.H.M., Rimmer, A., Lechinsky, Y., Wenker, K.J.R., Nussboim, S., van de Giesen, N.C., 2013. Measuring heat balance residual at lake surface using distributed temperature sensing. Limnol. Oceanogr. Methods 11 (1991), 79–90. http://dx.doi.org/10.4319/lom.2013.11.79.
Etemad-Shahidi, A., Faghihi, M., Imberger, J., 2010. Modelling thermal stratification and artificial destratification using DYRESM; case study: 15-Khordad reservoir. Int. J. Environ. Res. 4 (3), 395–406.
Falconer, R.A., George, D.G., Hall, P., 1991. Three-dimensional numerical modelling of wind-driven circulation in a shallow homogeneous lake. Journal of Hydrology 124, 59–79.
Fan, J., Furbo, S., 2012. Thermal stratification in a hot water tank established by heat loss from the tank. Sol. Energy 86 (11), 3460–3469.
Ferziger, J.H., Perić, M., 2002. Computational methods for fluid dynamics, third edition. Springer-Verlag, Berlin, Germany.
FLake, 2016. Lake Model FLake [online]. Available from: http://www.flake.igb-berlin.de/. [Accessed 8 November 2016].
Fluent, 2006. Natural Convection and Buoyancy-Driven Flows[online]. Available from http://aerojet.engr.ucdavis.edu/fluenthelp/html/ug/node572.htm. [Accessed 15 November 2016].
Fredriksson, S., 2011. A buoyantBoussinesqSurfactantFoam Tutorial: An Introduction to FAM. Technical Report. Chalmers University of Technology.
GARMIN, 2016. Etrex 20 [online]. Available from: https://buy.garmin.com/en-US/US/into-sports/discontinued/etrex-20/prod87771.html. [Accessed 14 November 2016].
Gianniou, S., Antonopoulos, V., 2007. Evaporation and energy budget in lake vegoritis, greece. J. Hydrol. 345 (3-4), 212–223. http://dx.doi.org/10.1016/j.jhydrol.2007.08.007.
Goff, J.A., 1957. Saturation pressure of water on the new kelvin temperature scale. Transactions of the American Society of Heating and Ventilating Engineers. pp. 347–354.
Google, 2015. Google Earth[online]. Available from https://www.google.com/earth/. [Accessed 20 November 2015].
Gooseff, M.N., Strzepek, K., Chapra, S.C., 2005. Modeling the potential effects of climate change on water temperature downstream of a shallow reservoir, lower madison river, MT. Clim. Change 68, 331–353.
Goudsmit, G.-H., Burchard, H., Peeters, F., Wuest, A., 2002. Application of $k-\varepsilon$ turbulence models to enclosed basins: the role of internal seiches. J. Geophys. Res. 107 (C12), 1–13. http://dx.doi.org/10.1029/2001JC000954.
Goula, A.M., Kostoglou, M., Karapantsios, T.D., Zouboulis, A.I., 2008. A CFD methodology for the design of sedimentation tanks in potable water treatment. Chem. Eng. J. 140 (1–3), 110–121.
Gschaider, B., 2015. groovyBC Boundary Condition[online]. Available from: https://openfoamwiki.net/index.php/Contrib/groovyBC. [Accessed 14 November 2016].
Gschaider, B., 2016. Swak4Foam[online]. Available from: https://openfoamwiki.net/index.php/Contrib/swak4Foam. [Accessed 14 November 2016].
Han, B.-P., Armengol, J., Carlos Garcia, J., Comerma, M., Roura, M., Dolz, J., Straskraba, M., 2000. The thermal structure of sau reservoir (NE: spain): a simulation approach. Ecol. Modell. 125, 109–122. http://dx.doi.org/10.1016/S0304-3800(99)00176-3.
Haque, M.M., Constantinescu, G., Weber, L., 2007. Validation of a 3D RANS model to predict flow and stratification effects related to fish passage at hydropower dams. J. Hydraul. Res. 45 (6), 787–796.
Henderson-Sellers, B., 1984. Development and application of a hydroclimate lake stratification model. Ecol. Modell. 21, 233–246.
Herb, W.R., Stefan, H.G., 2005. Dynamics of vertical mixing in a shallow lake with submersed macrophytes. Water Resour. Res. 41 (W02023), 1–14. http://dx.doi.org/10.1029/2003WR002613.
Hodges, B., Dallimore, C., 2014. Estuary, Lake and Coastal Ocean Model: ELCOM v3.0 User Manual. Center for Water Research, University of Western Australia, Australia.
Hodges, B.R., Imberger, J., Saggio, A., Winters, K.B., 2000. Modeling basin-scale internal waves in a stratified lake. Limnol. Oceanogr. 45 (7), 1603–1620. http://dx.doi.org/10.4319/lo.2000.45.7.1603.
Hondzo, M., Stefan, H., 1993. Lake water temperature simulation model. J. Hydraul. Eng. 119 (11), 1251–1273.
Idso, S.B., Gilbert, R.G., 1974. On the universality of the poole and atkins secchi disk-light extinction equation. J. Appl. Ecol. 11 (1), 399–401.
Kim, D.G., Cho, H.Y., 2006. Modeling the buoyant flow of heated water discharged from surface and submerged side outfalls in shallow and deep water with a cross flow. Environ. Fluid Mech. 6 (6), 501–518. http://dx.doi.org/10.1007/s10652-006-9006-3.
Kirillin, G., 2002. Modeling of the Vertical Heat Exchange in Shallow Lakes. Humboldt University of Berlin Thesis(PhD).
Kirillin, G., 2010. Modeling the impact of global warming on water temperature and seasonal mixing regimes in small temperate lakes. Boreal Environ. Res. 15, 279–293.
Koçyigit, M.B., Falconer, R.A., 2004. Three-dimensional numerical modelling of wind-driven circulation in a homogeneous lake. Adv. Water Resour. 27 (12), 1167–1178. http://dx.doi.org/10.1016/j.advwatres.2004.08.004.
Lap, B.Q., Mori, K., 2007. A two-dimensional numerical model of wind-induced flow and water quality in closed water bodies. Paddy Water Environ. 5, 29–40. http://dx.doi.org/10.1007/s10333-006-0063-5.
Laval, B., Imberger, J., Hodges, B.R., Stocker, R., 2003. Modeling circulation in lakes: spatial and temporal variations. Limnol. Oceanogr. 48 (3), 983–994.
Le Quéré, P., 1991. Accurate solutions to the square thermally driven cavity at high rayleigh number. Comput. Fluids 20 (1), 29–41. http://dx.doi.org/10.1016/0045-7930(91)90025-D.
Lee, H.S., Yamashita, T., Haggag, M., 2009. Modelling hydrodynamics in yachiyo lake using a non-hydrostatic general circulation model with spatially and temporally varying meteorological conditions. Hydrol. Process. 23, 1973–1987. http://dx.doi.org/10.1002/hyp.
Lee, I.-B., Bitog, J.P.P., Hong, S.-W., Seo, I.-H., Kwon, K.-S., Bartzanas, T., Kacira, M., 2013. The past, present and future of CFD for agro-environmental applications. Comput. Electron. Agric. 93, 168–183.
Lee, J.H., Bang, K.W., Choi, C.S., Lim, H.S., 2010. CFD modelling of flow field and particle tracking in a hydrodynamic stormwater separator. Water Sci. Technol. 62 (10), 2381–2388.
Lee, J.W., 2007. Numerical Modelling of Temperature-Induced Circulation in Shallow Water Bodies and Application to Torrens Lake, South Australia. The University of Adelaide Applied Mathematics Thesis(PhD). 10.1093/sp/2.2.123.
Lei, C., Patterson, J.C., 2001. Two- and three-dimensional temperature structures in a shallow wedge subject to solar radiation. 14th Australasian Fluid Mechanics Conference. pp. 359–362.
Lei, C., Patterson, J.C., 2002. Natural convection in a reservoir sidearm subject to solar radiation: a two-Dimensional simulation. Numer. Heat Transf., Part A 42, 13–32. http://dx.doi.org/10.1080/10407780290059404.
Liu, W.-C., Chen, W.-B., Chiu, C.-Y., 2012. Numerical modeling of hydrodynamic and hydrothermal characteristics in subtropical alpine lake. Appl. Math. Model. 36, 2094–2109. http://dx.doi.org/10.1016/j.apm.2011.08.011.
Livingstone, D.M., Imboden, D.M., 1989. Annual heat balance and equilibrium temperature of lake aegeri, switzerland. Aquat. Sci. 51 (4), 351–369.
Losordo, T.M., Piedrahita, R.H., 1991. Modelling temperature variation and thermal stratification in shallow aquaculture ponds. Ecol. Modell. 54, 189–226. http://dx.doi.org/10.1016/0304-3800(91)90076-D.
Maric, T., Hopken, J., Mooney, K., 2014. The openfoam technology primer, First edition. Sourceflux.
Markfort, C.D., Perez, A.L.S., Thill, J.W., Jaster, D.a., Porté-Agel, F., Stefan, H.G., 2010. Wind sheltering of a lake by a tree canopy or bluff topography. Water Resour. Res. 46, 1–13. http://dx.doi.org/10.1029/2009WR007759.
Marshall, J., Adcroft, A., Hill, C., Perelman, L., Heisey, C., 1997. A finite-volume, incompressible Navier Stokes model for studies of the ocean on parallel computers. J. Geophys. Res. 102 (C3), 5753–5766.
Massel, S.R., 1999. Fluid Mechanics for Marine Ecologists. Springer, Berlin, Germany.
MeshLab, 2016. MeshLab[online]. Available from: http://meshlab.sourceforge.net/. [Accessed 14 November 2016].

MITgcm, 2016. MITgcm (MIT General Circulation Model)[online]. Available from: http://mitgcm.org/. [Accessed 14 November 2016].
Momii, K., Ito, Y., 2008. Heat budget estimates for lake Ikeda, Japan. J. Hydrol. 361 (3–4), 362–370. http://dx.doi.org/10.1016/j.jhydrol.2008.08.004.
Naithani, J., Plisnier, P.-D., Deleersnijder, E., 2007. A simple model of the eco-hydrodynamics of the epilimnion of lake tanganyika. Freshw. Biol. 52, 2087–2100. http://dx.doi.org/10.1111/j.1365-2427.2007.01831.x.
Open Telemac-Mascaret Consortium, 2016. Open TELEMAC-MASCARET: the mathematically Superior Suite of Solver[online]. Available from: http://www.opentelemac.org/. [Accessed 8 November 2016].
OpenFOAM, 2016. CFD Direct: The Architects of OpenFOAM[online]. Available from: http://cfd.direct/. [Accessed 14 November 2016].
Politano, M., Haque, M.M., Weber, L.J., 2008. A numerical study of the temperature dynamics at mcnary dam. Ecol. Modell. 212, 408–421. http://dx.doi.org/10.1016/j.ecolmodel.2007.10.040.
QGIS, 2016. QGIS: A Free and Open Source Geographic Information System[online]. Available from: http://www2.qgis.org/en/site/. [Accessed 4 November 2016].
Raymarine, 2016. Experience Visionality with Dragonfly 6 and Dragonfly 7 Sonar GPS [online]. Available from: http://www.raymarine.com/view/?id=6855. [Accessed 14 November 2016].
Schertzer, W.M., Rouse, W.R., Blanken, P.D., Walker, A.E., 2003. Over-lake meteorology and estimated bulk heat exchange of great slave lake in 1998 and 1999. J. Hydrometeorol. 4 (4), 649–659.
Shih, T.-H., Liou, W.W., Shabbir, A., Yang, Z., Zhu, J., 1995. A new $k-\varepsilon$ eddy viscosity model for high reynolds number turbulent flows. Comput. Fluids 24 (3), 227–238.
Shufen, S., Jinfeng, Y., Xia, N., Changhai, S., 2007. Development of a model for water and heat exchange between the atmosphere and a water body. Adv. Atmos. Sci. 24 (5), 927–938. http://dx.doi.org/10.1007/s00376-007-0927-7.
Smith, R.C., Baker, K.S., 1981. Optical properties of the clearest natural waters (200–800 nm). Appl. Opt. 20 (2), 177–184.
snappyHexMesh, 2016. OpenFOAM User Guide: Mesh generation with snappyHexMesh [online]. Available from: http://cfd.direct/openfoam/user-guide/snappyhexmesh/. [Accessed 14 November 2016].
Subin, Z.M., Riley, W.J., Mironov, D., 2012. An improved lake model for climate simulations: model structure, evaluation, and sensitivity analyses in CESM1. J. Adv. Model. Earth Syst. 4, 1–27.
Svensson, U., 1998. PROBE: Program for Boundary Layers in the Environment (System description and Manual). NorrkÖping : Swedish Meteorological and Hydrological Institute.
Sweeney, D., 2004. Integrating Biological and Hydraulic Aspects of Waste Stabilisation Pond Design. Flinders University Thesis(PhD).
Ta, C.T., Brignal, W.J., 1998. Application of computational fluid dynamics technique to storage reservoir studies. Water Sci. Technol. 37, 219–226.
Tritton, D., 2007. Physical Fluid Dynamics. Clarendon Press, Oxford, United Kingdom.
Tsanis, I.K., 2006. Environmental hydraulics: Hydrodynamic and pollutant transport modelling of lakes and coastal waters. Elsevier, Amsterdam, Netherlands.
Verburg, P., Antenucci, J.P., 2010. Persistent unstable atmospheric boundary layer enhances sensible and latent heat loss in a tropical great lake: lake tanganyika. J. Geophys. Res. 115, 1–13. http://dx.doi.org/10.1029/2009JD012839.
Vercauteren, N., Huwald, H., Bou-Zeid, E., Selker, J.S., Lemmin, U., Parlange, M.B., Lunati, I., 2011. Evolution of superficial lake water temperature profile under diurnal radiative forcing. Water Resour. Res. 47, 1–10.
Verdier-Bonnet, C., Angot, P., Fraunie, P., Coantic, M., 1999. Three-dimensional modelling of coastal circulations with different $k-\varepsilon$ closures. J. Mar. Syst. 21, 321–339.
Vreugdenhil, C.B., 1994. Numerical Methods for Shallow-Water Flow, First. Kluwer Academic Publishers, Dordrecht, Netherlands.
Wang, J., Song, J., Huang, Y., Fan, C., 2013. On the parameterization of drag coefficient over sea surface. Acta Oceanolog. Sin. 32 (5), 68–74.
Wang, Y., 2013. Development of a Numerical Tool to Predict Hydrodynamics, Temperature and TDG in Hydropower Flows. University of Iowa Thesis(PhD).
White, F.M., 1991. Viscous Fluid Flow, Second edition. McGraw-Hill, New York, USA.
Williams, D.T., Drummond, G.R., Ford, D.E., Robey, D.L., 1981. Determination of light extinction coefficients in lakes and reservoirs. Proceedings of ASCE Symposium on Surface Water Impoundments. 1329–133
Wood, T.M., Cheng, R.T., Gartner, J.W., Hoilman, G.R., Lindenberg, M.K., Wellman, R.E., 2008. Modeling Hydrodynamics and Heat Transport in Upper Klamath Lake, Oregon, and Implications for Water Quality. Technical Report. U.S. Geological Survey.
Wüest, A., Lorke, A., 2003. Small-scale hydrodynamics in lakes. Annu. Rev. Fluid Mech. 35 (1), 373–412.
Yamashiki, Y., Kumagai, M., Jiao, C., Nezu, I., Matsui, S., 2003. Numerical simulation of thermally induced gyres in lake biwa. Hydrol. Process. 17, 2947–2956.
Yang, J., Wang, Z.-H., Li, Q., Vercauteren, N., Bou-Zeid, E., Parlange, M.B., 2016. A novel approach for unraveling the energy balance of water surfaces with a single depth temperature measurement. Limnol. Oceanogr. 00, 1–15.